Coordination Chemistry Reviews 253 (2009) 1906–1925

Contents lists available at ScienceDirect

Coordination Chemistry Reviews

journal homepage: www.elsevier.com/locate/ccr

Review

The coordination chemistry of 1,4,7,10-tetraazacyclododecane-N,N′,N″,N‴-tetraacetic acid (H_4DOTA): Structural overview and analyses on structure–stability relationships

Nerissa Viola-Villegas, Robert P. Doyle*

Department of Chemistry, Syracuse University, 1-014 Center for Science and Technology, Syracuse, NY 13244-4100, USA

Contents

1. Introduction 1907
2. Materials and methods 1909
3. Solid state structures 1909
   3.1. Class A structures (coordination number: 6 or 7) 1909
      3.1.1. Iron: Na[Fe(DOTA)·5H_2O] 1910
      3.1.2. Copper: Cu(H_2DOTA) 1910
      3.1.3. Gallium: [Ga(HDOTA)]·5.5H_2O; [Ga(H_2DOTA)]Cl 1910
      3.1.4. Nickel: Ni(H_2DOTA) 1913
      3.1.5. Cobalt: Co(H_2DOTA) 1913
      3.1.6. Zinc: Zn(H_2DOTA) 1913
   3.2. Class B DOTA derivatives (coordination number: 8 or 9) 1913
      3.2.1. Bismuth: Na[BiDOTA]•H_2O 1913
      3.2.2. Yttrium: Na[Y(DOTA)(H_2O)]·4H_2O 1913
      3.2.3. Gadolinium: Na[Gd(DOTA)(H_2O)]·H_2O 1914
      3.2.4. Europium: Na[Eu(DOTA)(H_2O)]·4H_2O 1915
      3.2.5. Thulium: K[Tm(DOTA)]·6H_2O·0.5KCl 1915
      3.2.6. Holmium: Na[Ho(DOTA)(H_2O)]·4H_2O 1916
      3.2.7. Dysprosium: Na[Dy(DOTA)(H_2O)]·Na(OH)·7H_2O 1916
      3.2.8. Lutetium: Na[Lu(DOTA)(H_2O)]·4H_2O 1916
      3.2.9. Neodymium: Na[Nd(DOTA)(H_2O)]·4H_2O 1917
      3.2.10. Praseodymium: Na[Pr(DOTA)(H_2O)]·4H_2O 1917
      3.2.11. Cerium: Na[Ce(DOTA)(H_2O)]·$NaHCO_3$·7H_2O 1917
      3.2.12. Lanthanum: Na[La(HDOTA)La(DOTA)]·10H_2O 1918
      3.2.13. Calcium: Ca(OH_2)$_3$[CaDOTA]·7.7H_2O 1918
      3.2.14. Strontium: {($C(NH_2)_3$)$_2$[Sr(DOTA)(H_2O)]}·4H_2O 1918
      3.2.15. Scandium: 3(Na[Sc(DOTA)])·NaOH·18H_2O 1918
4. Solid state structure in correlation to stability 1919
5. Summary 1923
   Acknowledgements 1924
   References 1924

Abbreviations: DOTA, 1,4,7,10-tetraazacyclododecane-N,N′,N″,N‴-tetraacetic acid; MRI, magnetic resonance imaging; PARACEST, paramagnetic chemical exchange transfer; EGFR, epidermal growth factor receptor; PRRT, peptide receptor radionuclide therapy; sstr, somatostatin receptor; toc, octreotide; tate, octreotate; lan, lanreotide; vap, vapreotide; PET, positron emission tomography; CSD, Cambridge Structural Database; C.N., coordination number.

* Corresponding author. Tel.: +1 315 443 3584; fax: +1 315 443 4070.
E-mail address: rpdoyle@syr.edu (R.P. Doyle).

0010-8545/$ – see front matter © 2009 Elsevier B.V. All rights reserved.
doi:10.1016/j.ccr.2009.03.013

Fusion Pharmaceuticals, Inc.
Exhibit 1035.001

ARTICLE INFO

Article history:
Received 29 August 2008
Accepted 11 March 2009
Available online 25 March 2009

Keywords:
DOTA
X-ray crystal structures
Structure–stability
Transition metals
Lanthanides

ABSTRACT

1,4,7,10-Tetraazacyclododecane-N,N′,N″,N‴-tetraacetic acid (DOTA) is one of the preeminent carriers of metal-based radiopharmaceutics and imaging contrast agents. This review focuses on the coordination chemistry of metal–DOTA complexes with a view to addressing the variability of structures obtained and gaining insight into its diversity. Correlations on thermodynamic stabilities with structural motifs are reported. Observed trends are analyzed with a view to providing a structure–stability relationship.

© 2009 Elsevier B.V. All rights reserved.

1. Introduction

1,4,7,10-Tetraazacyclododecane-1,4,7,10-tetraacetic acid or DOTA is a twelve-membered tetraazamacrocycle (see Fig. 1) containing four pendant carboxylate arms tethered to cyclen amines. Studies of metal complexes with DOTA have been reported since the 1980s with the first elucidated crystal structure of such complexes reported for Eu(III) in 1984 [1] and subsequently for Ni(II) and Cu(II) [2].

Work has been, and indeed continues to be driven by the medical imaging field with the need for a ligand possessing high thermodynamic stability and kinetic inertness in physiological conditions. Such properties are typical of DOTA complexes and have paved the way for metal-based magnetic resonance imaging agents (MRI) such as [Gd(DOTA)] for example. Studies by Naegele et al. reported the superiority of Gd(DOTA) through blood serum stability experiments and stability constant calculations [3]. The pharmacokinetic profile of this metal-ligand system then has resulted in prolific use in the field of MRI and has opened doors for research endeavors in metal-based pharmaceutics in general [4]. Work by Sherry et al. has led to derivatized DOTA complexes with a variety of applications. Aryl derivatives of the cyclen system complexed to Eu(III) were investigated by Sherry's group in an effort to make pH-dependent luminescent probes [5]. In addition, complexes of Eu(III) with DOTA containing tetraamide substituents are currently being explored for their efficiency as paramagnetic chemical exchange transfer (PARACEST) agents [5]. An application to this system via PARACEST utilizes Eu(III)–DOTA with *bis*(phenylboronate) pendant arms as an *in vivo* detector of glucose concentration (see Fig. 2a)

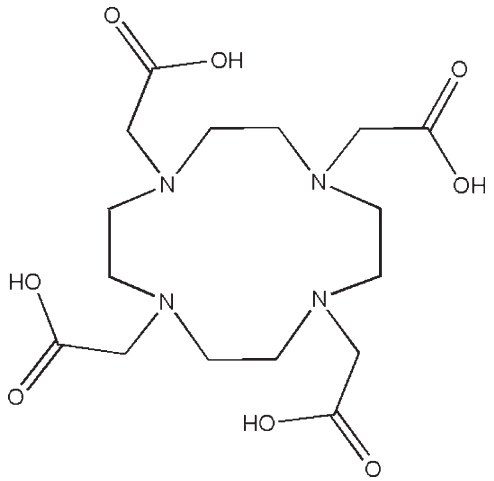


Fig. 1. The structure of 1,4,7,10-tetraazacyclododecane-N,N′,N″,N‴-tetraacetic acid (H_4DOTA).

[6]. PARACEST imaging is brought to new frontiers as more imaging agents are developed for the detection of a wide variety of enzymes and monitoring their activity [7–10]. One such endeavor involves ytterbium(III) complexed to a system composed of DOTA and β-D-galactopyranoside linked by a benzyloxycarbamate moiety as shown in Fig. 2b. The system utilizes the PARACEST effect to detect β-galactosidase and the kinetics of its cleavage reaction, an enzyme used for gene expression [11]. Other similar progress in PARACEST enzyme imaging centering on DOTA include detection of caspase-3 with thulium(III) [12].

The first report of studies employing ^{111}In (γ = 0.173 MeV and 0.247 MeV, $t_{1/2}$ = 67.2 h) [13] as an imaging agent was in 1990 when this radioisotope was chelated to a nitrobenzyl derivative of DOTA conjugated to a monoclonal antibody for target-specific radioimaging studies [14]. Decomplexation of indium in serum was monitored and it was observed that the rate loss of the metal was slower than with the use of other chelants [14]. This promising outcome paved the way for the numerous investigations utilizing ^{111}In-DOTA systems. The advent of radioimmunotherapy has seen a variety of antibody conjugates of DOTA being further explored [15–23,14]. In 1991, Lavender et al. initiated human clinical trials of ^{111}In-DOTA conjugated to the human IgG1 monoclonal antibody in seven patients, which resulted in successful tumor localization and imaging [19]. Another noteworthy radioimmunotherapy investigation targeted and illuminated breast cancers using the monoclonal chimeric antibody L6 with a peptide thiourea linker (see Fig. 3) and investigated the properties of ^{111}In- and ^{90}Y-DOTA with the radionuclides targeting the tumor with high specificity in contrast to bone marrow uptake [23].

Radioisotopes of copper complexed to DOTA have been widely explored and extensively used for illuminating tumors [24,25,18,26,22,27,28]. In 2002, $^{61/64}$Cu was labeled to DOTA with a marker for somatostatin, which resulted in enhanced uptake and microPET imaging contrast of pancreatic (AR42J) tumors in rat and mouse models [29]. A noteworthy study reported visualization of the stages of photodynamic therapy induced apoptosis in tumor-bearing mice using ^{64}Cu-DOTA conjugate of biotinylated streptavidin [25]. Results of this study provided a mechanistic insight on the apoptotic pathway taken by photosensitizers [25]. In 2008, Anderson et al. used DOTA conjugated to the anti-epidermal growth factor receptor (EGFR) antibody cetuximab and labeled with ^{64}Cu [18]. This radiopharmaceutical was observed to have localized in the nucleus of p53 positive EGFR overexpressing human colorectal cell line HCT116+/+ [18].

The versatility of DOTA has also seen its use in the field of peptide receptor radionuclide therapy (PRRT) [30,31]. Peptide vectors conjugated to the DOTA ligand (see Fig. 4) were used to target tumors that overexpress somatostatin receptors (SSTR) using different radioisotopes (e.g. ^{90}Y (β^- = 2.28 MeV, $t_{1/2}$ = 64.1 h) [17]; ^{68}Ga (β^+ = 2.92 MeV, $t_{1/2}$ = 67.6 min) [32]; ^{177}Lu (β^- = 0.497 MeV,

Fusion Pharmaceuticals, Inc.
Exhibit 1035.002

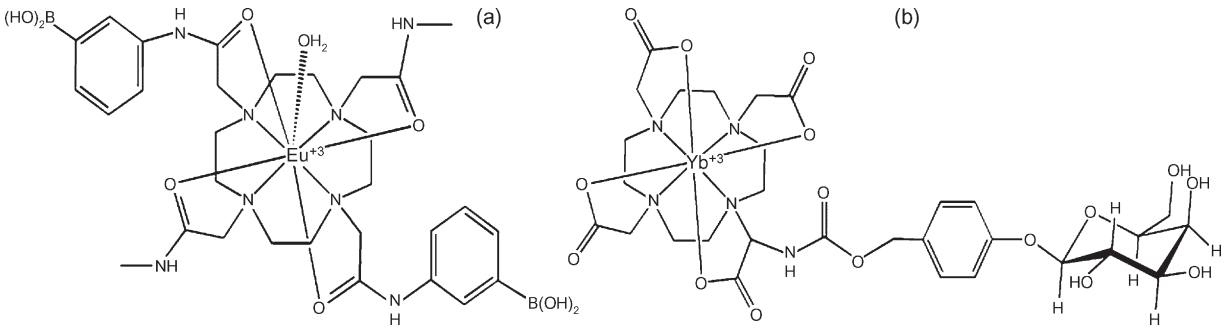


Fig. 2. (a) The structure of a PARACEST MRI contrast agent based on a europium complex of a tetraamide DOTA derivative with boronic acid substituents; (b) β-D-galactosidase PARACEST detector utilizing the paramagnetic properties of ytterbium chelated by a DOTA-β-D-galactopyranoside conjugate bridged by benzyloxycarbamate.

$t_{1/2}$ = 6.74 days) [33]). The first *in vivo* trials targeting the SSTR positive tumors of different histology evaluated ^{90}Y chelated to the system DOTATOC with post-injection of ^{111}In-DOTATOC to image the effects of the former radionuclide, which led to promising results [34]. The use of this β-particle emitter as a radiotherapy in twenty-nine patients resulted in a 67% disease stabilization with five patients developing renal/hematological toxicity [35]. Recent clinical trials employing this system towards metastatic medullary thyroid cancers gave low response rates [36], however, phase II clinical trials in patients with the same cancer resulted in longer survival rates of these patients [37].

Patients with lower tumor burden or those in the earlier stages of the disease are more responsive to treatment [36]. Further developments of ^{111}In with DOTALAN resulted in higher uptake compared to the octreotide derivative in neuroendocrine tumors, lymphomas and intestinal adenocarcinomas [38]. ^{177}Lu encapsulated in DOTA with a derivatized tyrosine-octreotate moiety is currently being explored as a low energy radionuclide therapy for SSTR positive tumors [39]. ^{68}Ga labeled DOTA remains to be the most promising radiotherapy as it provides a half-life of only 68 minutes and easily achieves blood clearance within a short duration [40]. A study conducted by Reubi et al. on binding affinities of peptide analogs of DOTA revealed a remarkable affinity of DOTATOC and DOTATATE labeled with cold gallium and ^{68}Ga to the SSTR subtype hsst2 in comparison to other trivalent metals (e.g. yttrium and indium) [41]. As a radiotracer, the physical properties of ^{68}Ga also make it suitable for positron emission tomography (PET). With the high affinity of gallium for SSTRs, high resolution PET imaging of small tumors in the neuroendocrine systems, which was unattainable with radiolabelled ^{111}In DOTA compounds, was recently achieved [42]. With ^{111}In-DOTATOC's limited ability to image smaller meningioma, ^{68}Ga-DOTATOC was explored as a PET tracer. This system displayed excellent imaging for small meningiomas (7–8 mm size) expressing SSTRs with high tumor-to-background ratio [43]. The variability in affinities towards the SSTRs was suggested to be a consequence of the structure of the drugs, its overall charge, hydrophilicity and even the coordination geometry of the metal–DOTA system [41]. Comparisons made among the radioisotopes ^{67}Ga, ^{111}In and ^{90}Y labeled DOTA conjugated to three different SSTR targeting derivatives (e.g. OC, TOC and TATE) resulted in better and improved tissue binding and internalization in pancreatic AR4-2J tumors for the ^{67}Ga radiolabelled ligand [44]. The first vitamin B9 conjugate of Ga(III) labeled DOTA was first reported by our group with a view to deliver the toxic metal to cancers upregulating the folate receptor. The stability of the metal in physiological conditions was not sufficient enough to achieve metal-induced cytotoxicity over 72 h. This system, however, is ideal for ^{68}Ga radiolabeling for PET imaging of these FR-overexpressing tumors [45].

Several reviews on metal–DOTA and DOTA derivatives have been reported [46,47]. These reviews focused on derivatized DOTA ligands and, in general, their application as radiopharmaceuticals. With the expanding use of this macrocyclic ligand in the medical research arena, we wanted to look into the relationship of the crystal structures and the stability H_4DOTA bestows on the complex. Serum stability studies of the radiopharmaceuticals reported rates of radiometal dissociation from different ligand systems including DOTA [48,49,15,50,22,51]. Thus, the stability of the cold isotopes plays a key role in our understanding of decomplexation rates to improve tropism and bioavailability of the metallodrug and prevent random tissue damage. However, there are few recent reviews integrating all metal–DOTA complexes with a view to analyzing the relationship between its solid state structures of solely DOTA and its metal system with their corresponding thermodynamic stability. There is, then a need to provide an overview of the coordination chemistry of solely H_4DOTA with the now greater than twenty such structures reported. With this important promise of

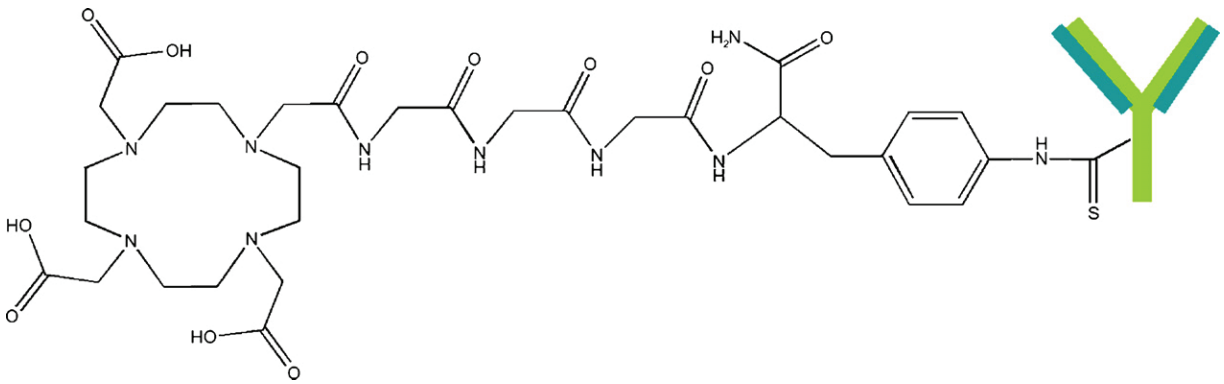


Fig. 3. The antibody chimeric L6 is conjugated to DOTA via a peptide thiourea linker formed by reaction of the isothiocyanate group of the bifunctional ligand with the primary amino group of the antibody (not shown).

Fusion Pharmaceuticals, Inc.
Exhibit 1035.003

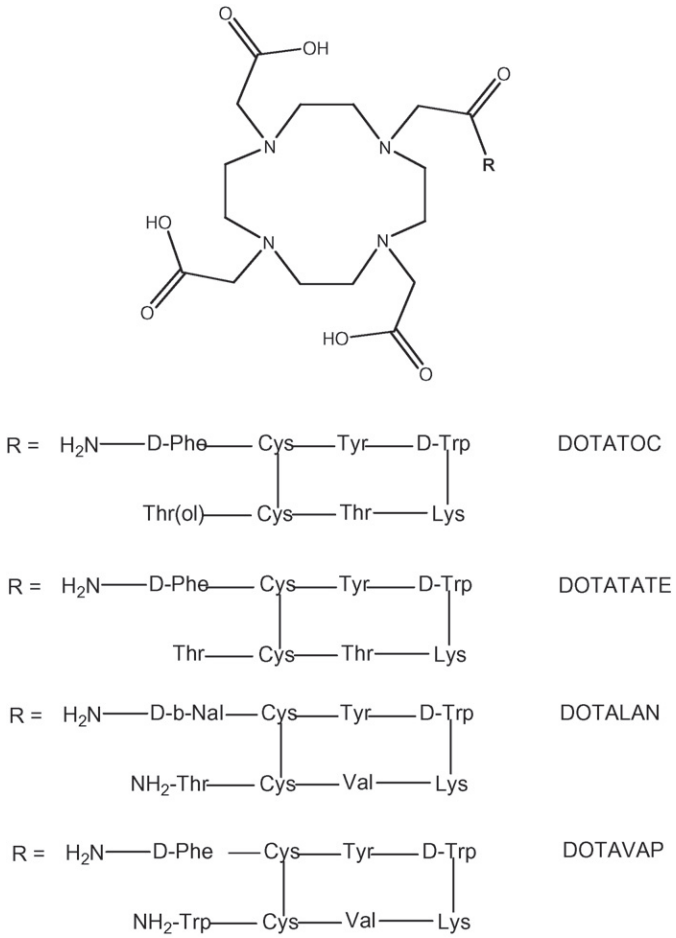


Fig. 4. DOTA-based peptide analogues utilized for PRRT (i.e. octreotide (DOTATOC), octreotate (DOTATATE), lanreotide (DOTALAN) and vapreotide (DOTAVAP)).

DOTA-based metal systems in medicine and the diverse array of coordination complexes formed, we have taken an in-depth look at the coordination chemistry of different metal–DOTA systems. Trends on bond lengths and angles, distance of the metal from the nitrogen and oxygen planes are described. Correlations of the solid-state structural properties to thermodynamic stability are provided.

This review will focus on the coordination chemistry of H_4DOTA only and its relationship to metal complexation stabilities. For the review of the different solid-state structures, the atom numbering assignments are retained according to literature. Each section contains DOTA systems ordered according to denticity. The metal systems for each section are arranged in the order of decreasing stability. It should be noted that the solid-state structures have different isomers but for our purposes, the molecular scheme represents only one isomer. The figures of the complexes and packing diagrams are chosen based on their unique and intriguing framework.

2. Materials and methods

Crystallographic data deposited beyond 1994 were obtained from the Cambridge Structural Database. Solid-state structures reported prior to 1994 were requested and obtained from the authors. Structural measurements were made using Mercury 1.4.2 software. Crystal structure images and packing structures were generated using CrystalMaker for Windows 1.4.5. Hydrogen bonds and lattice waters are omitted in the figures of the solid-state structures displayed.

3. Solid state structures

To our knowledge, only twenty-two complexes have been reported containing unmodified DOTA. An overview of the crystallographic and structural data is shown in Table 1. With DOTA possessing multidenticities and to aid in trend analysis, the solid-state structures of all reported metal–DOTA systems are categorized according to their coordination numbers. Class A crystals include hexa- and hepta-coordinate metal–DOTA derivatives, while Class B consists of crystal systems with coordination numbers 8 or 9.

3.1. Class A structures (coordination number: 6 or 7)

Table 2 lists detailed crystallographic data including selected bond lengths and angles of the metal–DOTA structures for Fe(III), Cu(II), Ga(III), Ni(II), Co(II) and Zn(II). For clarity and convention, the N_4-plane consists of the four nitrogen atoms in the cyclen ring.

Table 1
Crystallographic and structural data for coordinated DOTA systems ordered by space group.

Metal	Space group	Crystal System	Ionic radius, Å	Coordination number	DOTA donor set	Reference
Ga(III)	*C2/c*	Monoclinic	0.620	6	N_4O_2	[4]
Tm(III)	*C2/c*	Monoclinic	0.880	8	N_4O_4	[52]
Ca(II)	*C2/c*	Monoclinic	1.000	8	N_4O_4	[53]
Bi(III)	*C2/c*	Monoclinic	1.030	8	N_4O_4	[54]
Fe(III)	*Pna2₁*	Orthorhombic	0.645	7	N_4O_3	[55]
Ni(II)	*Pccn*	Orthorhombic	0.690	6	N_4O_2	[2]
Cu(II)	*Pccn*	Orthorhombic	0.730	6	N_4O_2	[2]
Co(II)	*Pccn*	Orthorhombic	0.745	6	N_4O_2	[56]
Zn(II)	*Pccn*	Orthorhombic	0.740	6	N_4O_2	[57]
Pr(III)	*P1̄*	Triclinic	0.850	9	N_4O_4	[52]
Lu(III)	*P1̄*	Triclinic	0.861	9	N_4O_4	[58]
Y(III)	*P1̄*	Triclinic	0.900	9	N_4O_4	[55], [59]
Ho(III)	*P1̄*	Triclinic	0.901	9	N_4O_4	[60]
Gd(III)	*P1̄*	Triclinic	0.938	9	N_4O_4	[55]
Eu(III)	*P1̄*	Triclinic	0.947	9	N_4O_4	[1]
Nd(III)	*P1̄*	Triclinic	0.983	9	N_4O_4	[52]
Ce(III)	*P2₁*	Monoclinic	1.020	9	N_4O_4	[52]
Sr(II)	*P4/ncc*	Tetragonal	1.180	9	N_4O_4	[61]
Dy(III)	*P2/c*	Monoclinic	0.912	9	N_4O_4	[52]
La(III)	*P2₁/n*	Monoclinic	1.032	9	N_4O_4	[62]
Ga(III)	*Cc*	monoclinic	0.620	6	N_4O_2	[56]
Sc(III)	*I4/m*	tetragonal	0.745	8	N_4O_4	[52]

Fusion Pharmaceuticals, Inc.
Exhibit 1035.004

Table 2
Crystallographic data for metal complexes of DOTA having a C.N. of 6 or 7.

Metal Formula Space group	Fe (III) Na[Fe(DOTA)] *Pna2₁*	Cu (II) Cu(H_2DOTA) *Pccn*	Ga(III) [Ga(HDOTA)]· 5.5 H_2O *C2/c*	Ga(III) [Ga(H_2DOTA)]Cl *Cc*	Co(II)	Ni(II) Ni(H_2DOTA) *Pccn*	Zn(II) Zn(H_2DOTA) *Pccn*
Z	4	4	8	4	4	4	4
a	8.764	9.444	22.732	15.171	15.225	9.280	9.384
b	18.618	15.300	16.015	14.962	9.392	15.248	15.294
c	14.382	13.109	12.9708	10.068	13.065	13.092	13.114
α	90.0	90.0	90.0	90.0	90.0	90.0	90.0
β	90.0	90.0	96.3	94.1	90.0	90.0	90.0
γ	90.0	90.0	90.0	90.0	90.0	90.0	90.0
Bond lengths							
N_{ax}–M	2.207	2.318	2.112	2.116	2.218	2.176	2.232
N_{ax}–M	2.353	2.107	2.137	2.187	2.218	2.113	2.171
N_{eq}–M	2.270	2.318	2.111	2.116	2.166	2.176	2.232
N_{eq}–M	2.269	2.107	2.133	2.105	2.166	2.113	2.171
O_{eq}–M	2.044	1.966	1.929	1.913	2.034	2.025	2.037
O_{eq}–M	2.047	1.966	1.940	1.940	2.034	2.025	2.037
O_3–M	2.059	n.a.	n.a.	n.a.	n.a.	n.a.	n.a.
Bond angles							
O_1–M–O_2	83.94	88.07	85.30	82.40	90.89	86.90	89.71
O_2–M–O_3	79.95	n.a.	n.a.	n.a.	n.a.	n.a.	n.a.
O_2–M–O_4	78.14	n.a.	n.a.	n.a.	n.a.	n.a.	n.a.
N_1–M–N_2	77.56	82.31	82.03	83.62	82.38	82.98	81.89
N_2–M–N_3	73.45	81.09	84.19	84.41	82.30	84.88	82.84
N_1–M–N_3	124.07	152.59	156.48	157.14	153.77	158.36	153.92
N_2–M–N_4	124.44	104.96	107.70	108.94	108.08	108.59	107.83
N_1–M–N_4	81.10	82.31	82.90	82.00	82.38	82.98	81.89
N_3–M–N_4	77.40	81.09	83.26	83.51	82.38	84.44	82.84
Metal–plane displacement							
N_4 plane	1.06	0.92	0.84	0.83	0.89	0.82	0.89
O_4 plane	1.36	n.a.	n.a.	n.a.	n.a.	n.a.	n.a.

3.1.1. Iron: Na[Fe(DOTA)·5H_2O

The DOTA complex of Fe(III) with the molecular formula {Na[Fe(DOTA)]·5H_2O} results in a seven-coordinate Fe(III) [55], a rare occurrence for Fe(III) coordination complexes [63] (see Fig. 5).The Fe(III) center is coordinated to the four nitrogen atoms of the cyclen ring and three oxygen atoms from the carboxylate arms leaving the fourth carboxylate DOTA arm free to hydrogen bond to water molecules [55]. The M–N bond lengths range from 2.200–2.353 Å with the longer bond resulting from steric hindrance [55]. Bond distances for Fe(III)–O are in the range of 2.044–2.059 Å. The angles formed (N–M–N) between *cis* nitrogen atoms are 73.45°, 77.4°, 77.56° and 81.1° and those *trans* to each other are ∼124°. The distance of the metal from the N_4-plane formed by the four amines is 1.058 Å.

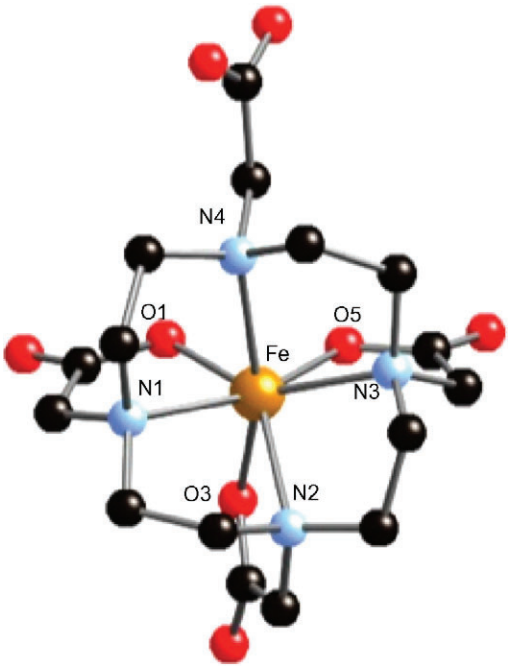


Fig. 5. Coordination geometry of Na[Fe(DOTA)]·5H_2O showing a seven-coordinate Fe(III) viewed along the crystallographic *xy* plane. Hydrogen atoms and lattice waters are omitted for clarity.

3.1.2. Copper: Cu(H_2DOTA)

Copper(II) is coordinated to DOTA through its four nitrogen atoms and two oxygen atoms from the carboxylic arms [2]. The two other pendant arms are protonated and do not participate in coordination. Two of the Cu–N bonds found at axial positions are longer than normal at 2.318 Å as an effect of Jahn-Teller expansion. The equatorial Cu–N bond lengths are observed to be 2.107 Å. The bond distances for Cu–O are equivalent at 1.966 Å. The carboxylate groups found coordinated to the metal center are attached to the equatorial amines. The O–Cu–O angle is determined to be 88.07°. Two angles formed by N–Cu–N are equivalent with *cis* nitrogen atoms at 82.31° and 81.09° while the *trans* nitrogen-metal bond angles are at 152.59° and 104.96°. Copper(II) is displaced from the N_4-plane by a distance of 0.916 Å [2].

3.1.3. Gallium: [Ga(HDOTA)]·5.5H_2O; [Ga(H_2DOTA)]Cl

The molecular structure of [Ga(HDOTA)]·5.5H_2O (see Fig. 6) reported in 2006 is hexacoordinate, monoclinic and crystallizes under the space group *C2/c*. Gallium(III) is coordinated to the nitrogen atoms of the DOTA ring and two oxygen atoms from the carboxyl arms [4]. Bond lengths for Ga–N as well as for Ga–O are shorter than normal ranging from 2.111–2.137 Å and a mean of 1.93 Å respectively. A bond angle of 85.3° is formed with respect to the coordinating oxygen atoms and gallium. The

Fusion Pharmaceuticals, Inc.
Exhibit 1035.005

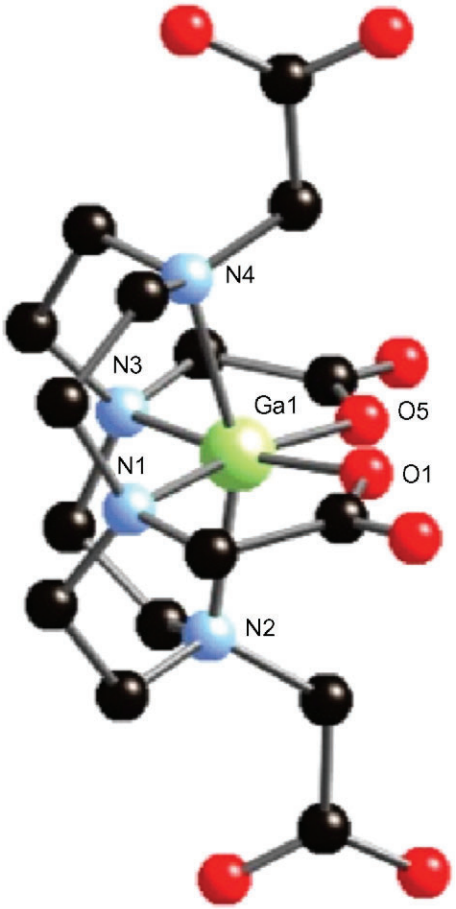


Fig. 6. The molecular structure of [Ga(HDOTA)·5.5H_2O] viewed along the crystallographic *z*-axis. Hydrogen atoms and lattice waters are omitted for clarity.

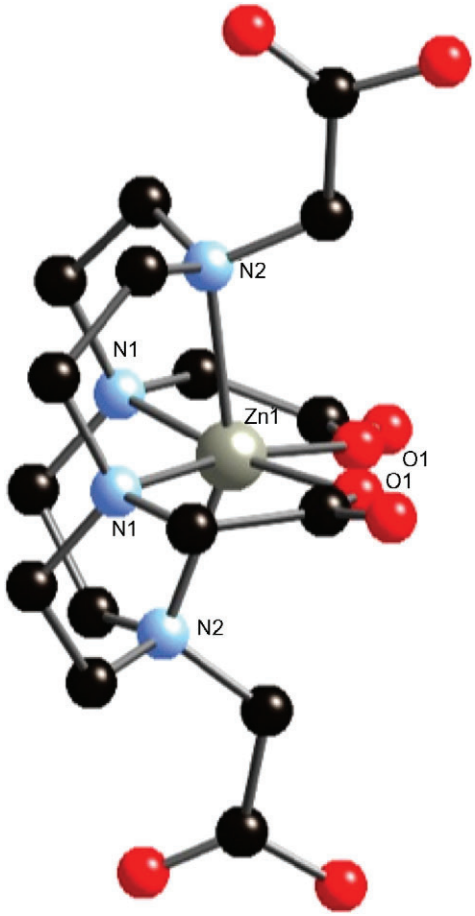


Fig. 8. A hexacoordinate [Zn(H_2DOTA)] complex showing a distorted octahedron viewed down the *y*-crystallographic axis. Hydrogen atoms are omitted for clarity.

angles formed by *cis*- nitrogen atoms and gallium ranges from 82.03° to 84.19°. *Trans* axial nitrogen atoms display an observed 156.48° and 107.70° with the metal center suggesting a distorted octahedral. Gallium(III) is puckered from the N_4-plane by a distance of 0.84 Å. The two other remaining uncoordinated arms are unique as one remains a carboxylic acid while the other arm is deprotonated. This is demonstrated by the angle produced by C12–O3–H3 (109.4°), which is consistent with a tetrahedral geometry.

This gallium derivative of DOTA packs in an asymmetric ABAB motif as shown in Fig. 7a when viewed down the crystallographic *z*-axis. This system packs with each unit connected via intermolecular hydrogen-bonding of lattice water molecules with the uncoordinated carboxylate arms. This bridging pattern forms a polymeric one-dimensional chain structure.

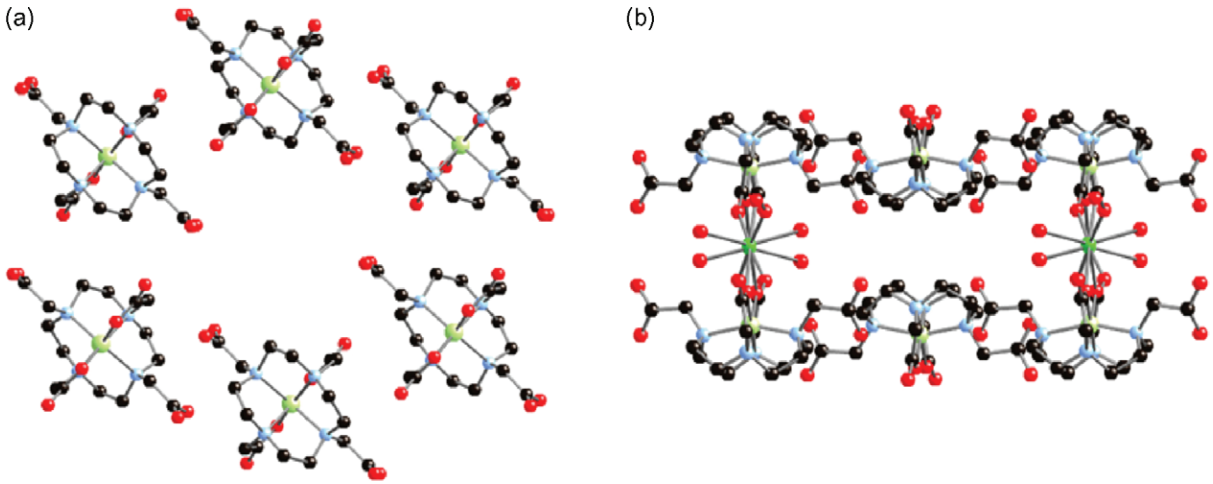


Fig. 7. (a) Ga(HDOTA)·5.5H_2O packs in an ABAB layer as viewed down the crystallographic *z*-axis; (b) [Ga(H_2DOTA) (Cl)] packing scheme as viewed through the *z*-axis shows interaction between units through a chlorine atom.

Fusion Pharmaceuticals, Inc.
Exhibit 1035.006

Table 3
Crystallographic data of 8 or 9 coordinate DOTA systems.

Metal Formula	Ca(II) $Ca(OH_2)_3$ [CaDOTA] $\cdot 7.7H_2O$	Sr(II) $[C(NH_2)_3]_2$ [Sr(DOTA) (H_2O)]	Bi(III) NaBiDOTA. H_2O	Y (III) Na[Y(H_2O) (DOTA)]	Sc(III) 3(Na[Sc(DOTA))· NaOH· $18H_20$	La(III) Na[La(HDOTA) La(DOTA)]· $10H_2O$	Ce (III) Na[Ce(DOTA) (H_2O)]. $NaHCO_3.7H_2O$	Pr (III) Na[Pr(DOTA) H_2O)].$4H_2O$	Nd (III) Na[Nd(DOTA) (H_2O)]·$4H_2O$	Dy (III) Na[Dy(DOTA) (H_2O)]· NaOH.$7H_2O$	Ho (III) Na[Ho(DOTA) (H_2O)]·$4H_2O$	Lu (III) Na[Lu(DOTA) (H_2O)]·$4H_20$	Tm(III) K[Tm(DOTA)]· $6H_2O$·0.5KCl	Eu (III) Na[Eu(DOTA) (H_2O)]·$4H_2O$	Gd (III) Na[Gd(H_2O) (DOTA)] ·$4H_2O$
Space group	*C2/c*	*P4/ncc*	*C2/c*	*Pī*	*I4/m*	$P2_1/n$	$P2_1$	*Pī*	*Pī*	*P2/c*	*Pī*	*Pī*	*C2/c*	*Pī*	*Pī*
Z	8	4	4	2	16	4	2	2	2	4	2	2	8	2	2
a	25.109	12.82	17.053	8.752	12.517	16.425	9.04	8.715	8.705	12.17	8.735	8.732(2)	37.55	8.734	8.711
b	18.557	n.a.	6.587	9.097	12.517	11.942	9.024	9.188	9.16	8.977	9.093	9.035(3)	8.981	9.116	9.111
c	18.436	18.501	20.048	15.625	48.015	25.384	18.266	15.88	15.84	27.891	15.64	15.518(3)	16.783	15.773	15.625
α	90	90	90	82.94	90	90	90	82.74	82.77	90	82.94	82.96	90	82.83	82.94
β	134.85	90	102	85.88	90	94.75	92	84.93	85.05	99.88	85.85	86.37	111.09	85.34	85.88
γ	90	90	90	81.61	90	90	90	80.98	81.09	90	81.76	81.79	90	81.43	81.61
Bond lengths															
N1–M	2.597, 2.571	2.732	2.516	2.635	2.444	2.751, 2.805	2.73	2.724	2.727	2.638	2.627	2.597	2.519	2.664	2.656
N2–M	2.615, 2.581	2.732	2.535	2.666	2.444	2.781, 2.797	2.744	2.703	2.693	2.632	2.642	2.621	2.532	2.704	2.688
N3–M	2.597, 2.571	2.732	2.516	2.633	2.444	2.759, 2.792	2.69	2.746	2.704	2.612	2.632	2.597	2.534	2.66	2.645
N4–M	2.615, 2.581	2.732	2.535	2.648	2.444	2.788, 2.783	2.766	2.711	2.689	2.61	2.664	2.64	2.531	2.677	2.661
M–O1	2.420, 2.376	2.548	2.495	2.327	2.147	2.486, 2.479	2.462	2.43	2.406	2.325	2.322	2.279	2.269	2.372	2.379
M–O2	2.434, 2.440	2.548	2.58	2.324	2.147	2.483, 2.479	2.462	2.439	2.42	2.344	2.331	2.285	2.288	2.38	2.362
M–O3	2.420, 2.376	2.548	2.495	2.316	2.147	2.490, 2.508	2.442	2.437	2.426	2.329	2.336	2.269	2.278	2.39	2.359
M–O4	2.434, 2.440	2.548	2.58	2.324	2.147	2.509, 2.507	2.472	2.419	2.413	2.352	2.33	2.282	2.282	2.373	2.37
M–Ow	n/a	2.849	n.a.	2.435	n.a.	n.a.	2.598	2.53	2.508	2.479	2.443	2.416	n.a.	2.484	2.463
Bond Angles															
O1–M–O2	79.71	84.12	79.68	81.7	77.29	80.56, 80.64	84.57	87.72	87.6	84.29	81.42	83.3	78.49	81.89	87
O2–M–O3	76.8	84.12	78.18	86.81	77.29	90.12, 89.20	84.98	84.58	82.46	84.32	85.67	81.5	77.21	86.48	81.87
O2–M–O4	126.06	142.66	126.69	143.12	124.04	147.88, 146.19	144.98	146.83	148.23	143.06	142.58	143.3	124.72	146.32	143.74
O1–M–O3	126.68	142.66	129.31	144.84	124.04	146.58, 145.24	143.54	149.09	145.95	141.56	144.59	141.7	123.96	144.13	145.92
O3–M–O4	79.71	n.a.	n.a.	85.77	77.29	83.06, 84.34	83.7	87.51	87.21	84.18	83.77	86.4	76.51	84.02	86
O4–M–O1	76.8	n.a.	n.a.	83.8	77.29	88.04, 86.22	85.14	82.75	84.45	83.26	86.76	85.14	77.46	87.15	72
N1–M–N2	69.33, 70.14	66.19	71.20	67.6	72.84	64.41, 64.52	65.08	66.85	67.11	68.84	67.86	69.1	69.63	67.42	67.53
N2–M–N3	69.32, 69.46	66.19	71.19	67.8	72.84	64.64, 64.75	65	67.68	67.15	68.72	67.9	68	70.65	67.99	67.7
N1–M–N3	106.79, 107.98	101.1	110.69	104.7	114.19	97.85, 98.16	100.13	102.81	103.46	105.15	104.98	105.2	109.1	104.1	104.3
N2–M–N4	107.38, 108.17	101.1	110.93	104.6	114.19	97.94, 98.62	98.92	103.02	103.28	106.16	105.04	105.4	109.13	104.2	104.4
N1–M–N4	69.33, 70.14	66.19	71.20	68.8	72.84	64.37, 65.32	65.13	67.13	67.96	67.92	68.41	68.3	70.76	68.24	68.5
N3–M–N4	69.32, 69.46	66.19	71.20	68.2	72.84	64.38, 65.32	66.16	66.96	67.36	68.87	68.85	68.3	70.37	67.57	68
O1–M–Ow	n.a.	71.33	n.a.	72.1	n.a.	n.a.	67.88	74.58	74.09	71.6	69.05	68.77	n.a.	73.02	73.28
O2–M–Ow	n.a.	71.33	n.a.	72.88	n.a.	n.a.	73.49	70.59	75.84	71.55	72.86	71.41	n.a.	74.62	74.32
O3–M–Ow	n.a.	71.33	n.a.	69.29	n.a.	n.a.	75.65	74.63	70.12	69.96	71.88	72.92	n.a.	73.44	72.8
O4–M–Ow	n.a.	71.33	n.a.	73.83	n.a.	n.a.	71.54	76.26	74.26	71.52	73.53	72.04	n.a.	69.51	69.42
Metal–Plane Displacement															
N_4 plane	1.549	1.736	1.736	1.616	1.434	1.835, 1.810	1.765	1.695	1.676	1.585	1.608	1.586	1.466	1.645	1.632
O_4 plane	1.095	0.816	0.816	0.718	1.112	0.702, 0.728	0.604	0.671	0.684	0.755	0.727	0.732	1.064	0.71	0.715

Fusion Pharmaceuticals, Inc.
Exhibit 1035.007

A second gallium-DOTA complex structure was elucidated by the group of Maecke in 2008 [56]. The crystals were grown in a basic pH (~8.0) compared to a pH of 4.8 for the original 2006 structure, and possess a *Cc* crystallographic space group. The two crystal structures differ not only in space group but in the pendant side arms and in packing schemes (see Fig. 7b). Both uncoordinated carboxyl arms in the latter structure are protonated whereas the first crystal structure possesses both deprotonated and protonated arms. The crystal packing of the latter gallium structure displays bridging of molecular units through carbonyl oxygen atoms coordinated to a chlorine atom whereas the first gallium complex of DOTA interacts with another unit through hydrogen-bonding.

3.1.4. Nickel: Ni(H_2DOTA)

Ni(H_2DOTA) produces a slightly distorted octahedral Ni(II) geometry, with two oxygen atoms from the carboxylate arms and all nitrogen atoms from the macrocycle coordinated to the Ni(II) center. The Ni–N bond distances range from 2.113–2.176 Å. The Ni–O bond lengths are equivalent at 2.025 Å. The bond angle formed between the coordinating oxygen atoms and the metal ion is ~86.9°. Two of the angles formed by nitrogen atoms *cis* to each other are equivalent at 82.98° while the other two angles differ by 0.44° at 84.44° and 84.88°. The two *trans* nitrogen bond angles include 158.36° and 108.59°. Metal displacement from the N_4-plane was measured to be 0.821 Å [2].

3.1.5. Cobalt: Co(H_2DOTA)

Cobalt complexes are widely explored for their ability to induce apoptosis via oxidative stress as a result of their redox activity. Cobalt cyclen compounds have been widely studied for their ability to cut phosphodiester bonds [64,65] and peptides [66,67]. A solid state structure of the cobalt–DOTA system has been recently reported. It displays a similar *Pccn* crystallographic space group as found with the Cu(II) [2], Ni(II) [2] and Zn(II) [57] derivatives. It is hexacoordinate with the two nitrogen amines (~2.218 Å) bound at the axial positions. While the other two nitrogen atoms (~2.166 Å) of the cyclen ring and two carboxyl oxygen atoms (~2.034 Å) are coordinated at the equatorial sites of the octahedron. Bond angles formed by the equatorial N_2O_2 donor set are consistent with the range observed for this class (O–M–O ~ 78–91°; *cis* N–M–N ~ 73–85°; *trans* N–M–N ~ 104–159°).

3.1.6. Zinc: Zn(H_2DOTA)

The molecular structure is shown in Fig. 8. The zinc derivative crystallizes in the orthorhombic *Pccn* space group with $Z = 4$ [57]. This compound is similar to the copper(II) and nickel(II) complexes of DOTA. The zinc atom is bound to the six different donor sites of the ligand: four nitrogen atoms from the cyclen ring and two oxygen atoms from the carboxylic acid groups. The two Zn–O bonds formed are both 2.037 Å in length with the Zn–N bonds longer at 2.232 Å and 2.171 Å. The N–Zn–N angles with the nitrogen atoms *trans* to each other are 153.92° and 107.83°. Bond angles for the *cis* nitrogen atoms and the metal center range from 81.89–82.82°. This only shows that the structure is distorted with the bond angles less than the ideal octahedral angles of 180° and 90°. The metal is slightly displaced from the N_4-plane by 0.891 Å.

3.2. Class B DOTA derivatives (coordination number: 8 or 9)

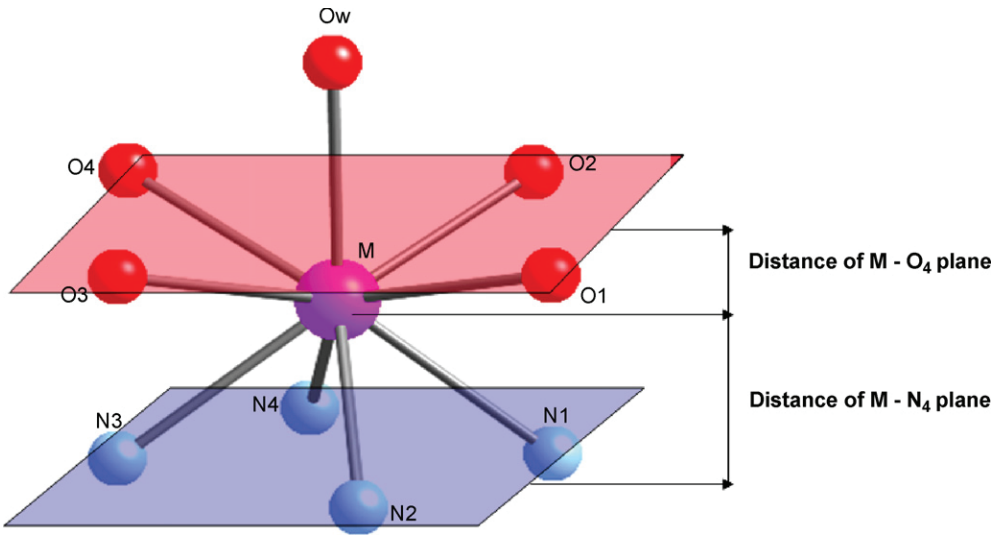
Crystallographic data for class B DOTA derivatives are listed in Table 3. Two planes are formed by the N_4 and O_4 donor sets as shown in Scheme 1.

3.2.1. Bismuth: Na[BiDOTA]•H_2O

Na[BiDOTA]·H_2O was observed to crystallize in the centrosymmetric space group *C2/c*. The structure was determined to be eight coordinate with all four nitrogen atoms and oxygen atoms bound to the metal center. Hence, the molecular structure is square antiprismatic [54]. The mean bond lengths for N–Bi and O–Bi are 2.525 Å and 2.5375 Å respectively. *Cis* bond angles formed by O–Bi–O range from 78.18°–79.68°. The largest O–Bi–O angles formed between *trans* oxygen atoms are typically 26.69°–129.31°. For the nitrogen atoms, the bond angles average at 71.2° and 110.8°. Bismuth is displaced from the O_4-plane by 1.112 Å and the N_4-plane by 1.434 Å. Each crystal unit of this DOTA analog is indirectly interacting with each other through sodium adducts. Each sodium atom is coordinated to a carboxyl group of the macrocycle and solvent water molecules. The sodium atoms are connected by water molecules. This bridges the Bi-DOTA units into one-dimensional polymeric chains as displayed in Fig. 9.

3.2.2. Yttrium: Na[Y(DOTA)(H_2O)]·4H_2O

The anionic [Y(DOTA)(H_2O)]$^-$ acts as a nine-coordinate system having the crystallographic space group *P*$\bar{1}$ [55,59]. All four nitrogen donors along with the oxygen atoms from the carboxyl groups



Scheme 1. Diagram of class B DOTA systems showing two planes with O_4-plane (red) containing O_1, O_2, O_3 and O_4 and N_4-plane (blue) formed by N_1, N_2, N_3 and N_4 and their distances from the metal center.

Fusion Pharmaceuticals, Inc.
Exhibit 1035.008

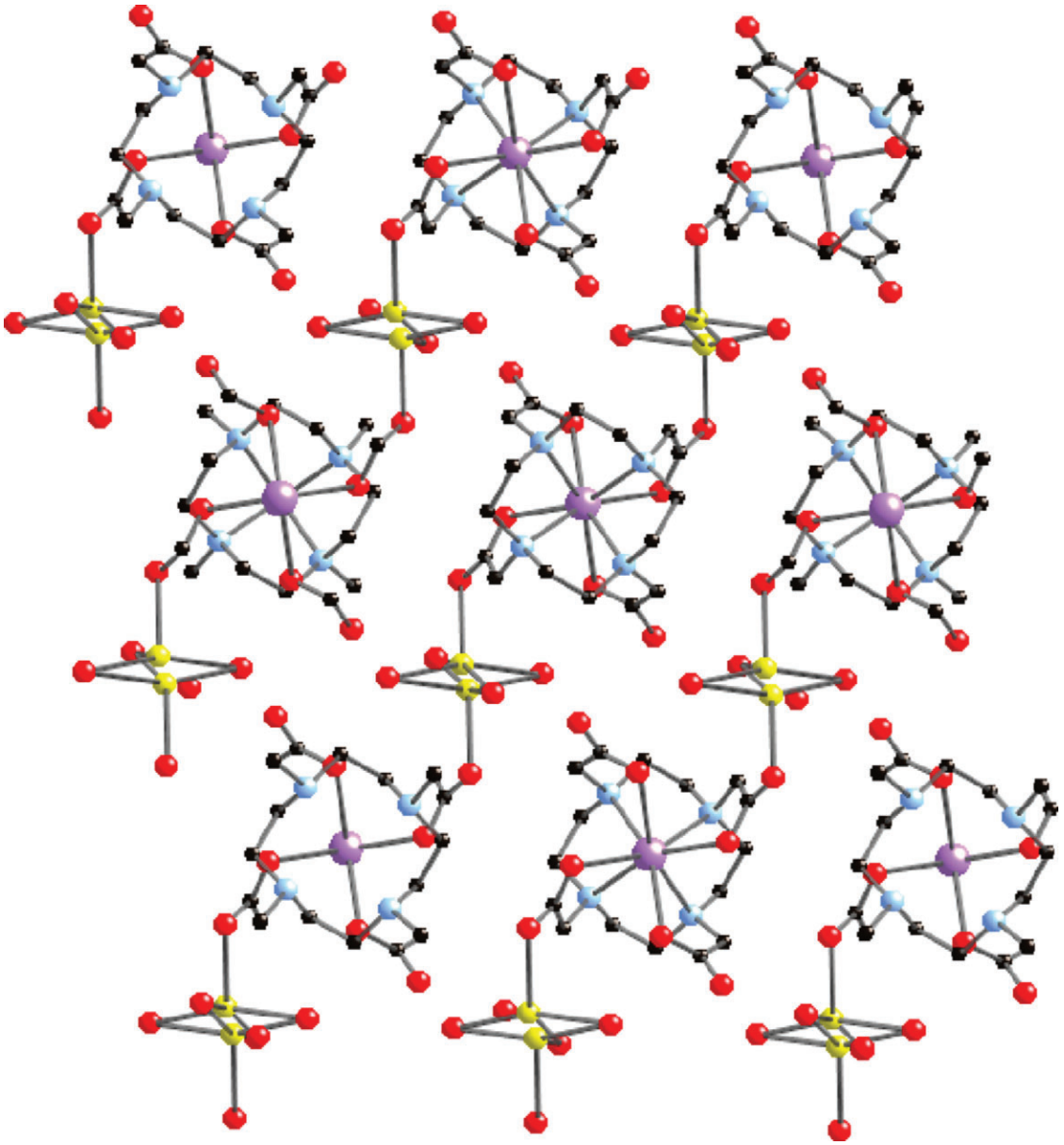


Fig. 9. The packing structure of Na[BiDOTA]·H_2O shows units bridged by sodium atoms along the *y*-axis.

are coordinated to the metal center. The oxygen (O5) from water serves as a capping ligand to complete the square antiprismatic geometry (see Fig. 10). The N-donors are spaced within the range of 2.633–2.648 Å from the metal.

The O-donors are typically 2.316–2.327 Å from yttrium. The Y–O5 bond, however, is longer with a distance of 2.435 Å. This molecule packs two units in a unit cell with sodium as the bridging cation. The O–Y–O bond angles range from 81.70°–86.81°. The angles formed by N–Y–N are narrower at 67.7–68.8°. Yttrium is displaced from the N_4-plane by 1.616 Å and from the O_4-plane by 0.718 Å.

3.2.3. Gadolinium: Na[Gd(DOTA)(H_2O)]·H_2O

X-ray diffraction studies of a single crystal of Na[Gd(DOTA)(H_2O)]·4H_2O revealed its crystallographic space group to be $P\bar{1}$. The nine-coordinate structure is square antiprismatic with all N- and O-donor sets coordinated to Gd(III). The ninth coordination site is occupied by water, the capping ligand (see Fig. 11). This derivative of the DOTA system is isostructural with

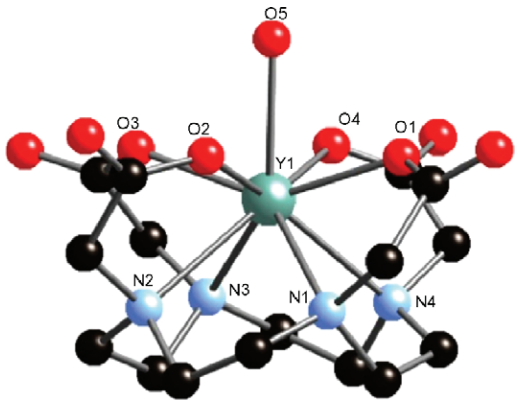


Fig. 10. The molecular structure of {Na[Y(H_2O)(DOTA)]} showing a square antiprismatic geometry viewed down the crystallographic *y*-axis. Hydrogen atoms are omitted for clarity.

Fusion Pharmaceuticals, Inc.
Exhibit 1035.009

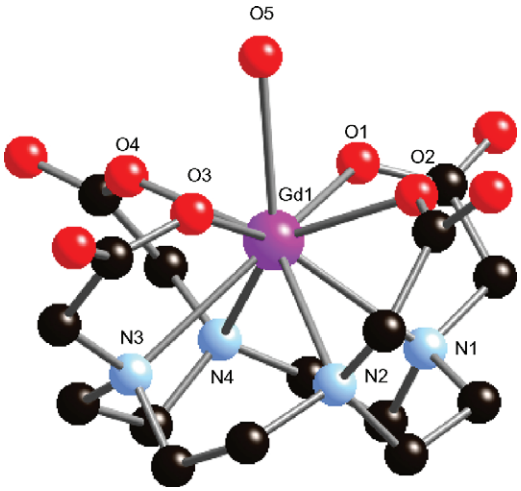


Fig. 11. The nine-coordinate molecular structure of Na[Gd(DOTA)(H_2O)]·H_2O as viewed along the crystallographic *xy* plane. Hydrogen atoms and lattice waters are omitted for clarity.

other enneacoordinate metal–DOTA systems (i.e. Y(III), Ce(III), Nd(III), Pr(III), Eu(III), Dy(III), Ho(III), Lu(III)). The Gd–N and Gd–O bond lengths are within the observed range of bond lengths for both donor sets with an average of ~2.66 Å and 2.27 Å respectively. The bond angles formed by *cis* nitrogen donors (N–Gd–N) with the smallest and largest angle vary by 1°. The *cis* oxygen donors form angles with Gd(III) with a higher deviation (e.g. 72.0°, 81.9°, 86.0° and 87.0°). The displacements of the metal from the N_4 (1.632 Å) and O_4 (0.715 Å) plane fall within the range of the determined metal-plane distances.

3.2.4. *Europium: Na[Eu(DOTA)(H_2O)]·$4H_2O$*

The first crystal of a metal–DOTA complex, Na[Eu(DOTA)(H_2O)]·$4H_2O$, is colorless and grew over time via slow evaporation [1]. X-ray diffraction experiments determined that this macrocyclic europate is triclinic with a crystallographic space group of $P\bar{1}$. The DOTA ligand encapsulates the Eu(III) atom and with an aquo ligand forms a nine-coordinate structure. The Eu(III) atom forms a distorted capped square antiprism. The four nitrogen atoms are coordinated to the Eu(III) atom with a mean distance of ~2.68 Å. The Eu–O bonds formed by the carboxylate arms are noticeably shorter than the Eu–N bonds and range from 2.37 Å to 2.39 Å. The distance of Eu(III) from the N_4 plane is measured to be 1.645 Å. In

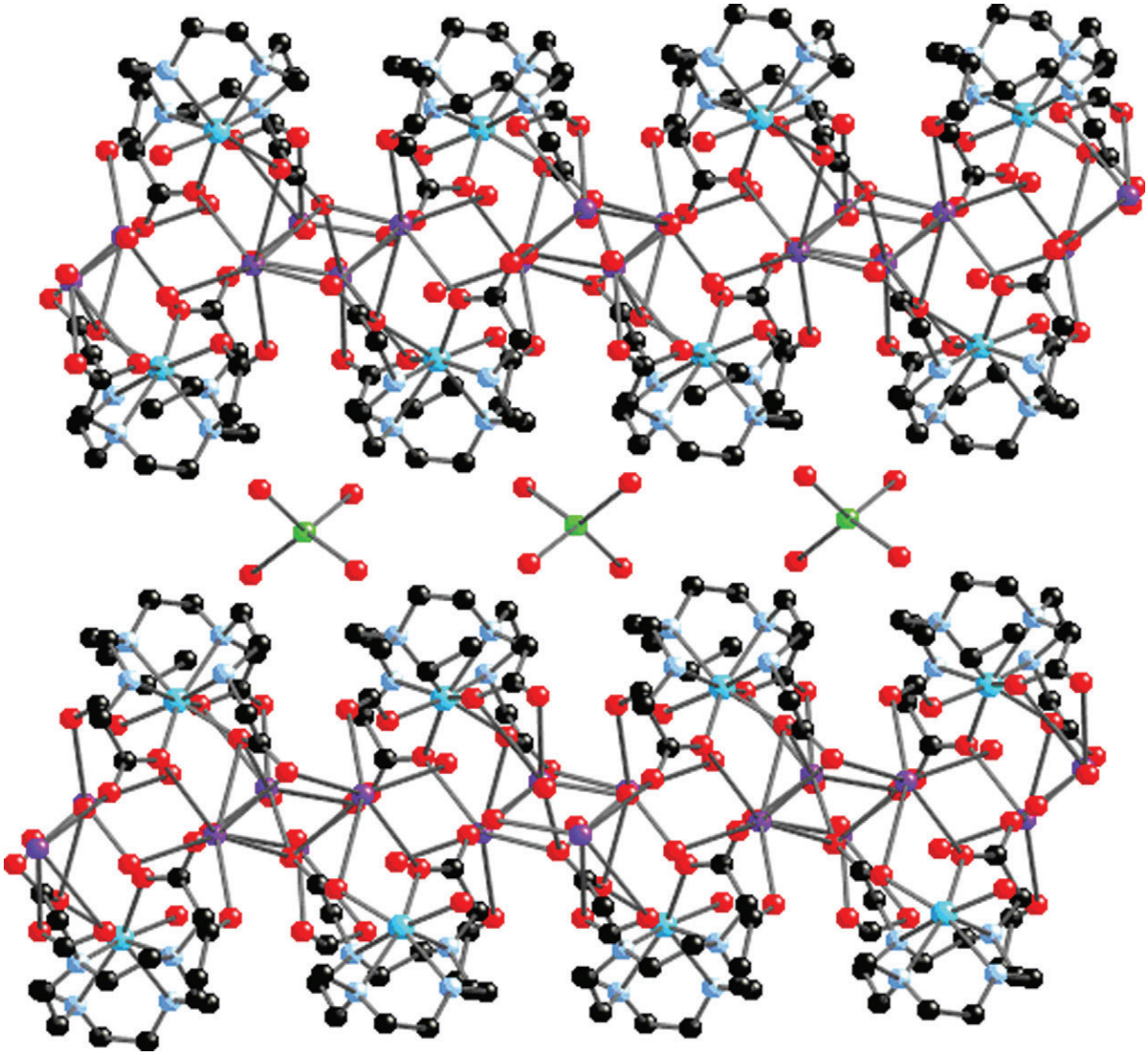


Fig. 12. The packing diagram of Tm(III) complexed to DOTA viewed along the *y*-axis.

Fusion Pharmaceuticals, Inc.
Exhibit 1035.010

addition, the Eu(III) metal center is situated just 0.718 Å from the oxygen plane. Monocapping of the coordination sphere with the aquo ligand provided a Eu–Ow distance of 2.84 Å.

3.2.5. Thulium: K[Tm(DOTA)]·6H_2O·0.5KCl

Among the solid-state structures of the lanthanide-DOTA systems, the crystal of thulium encapsulated by DOTA is one of the rare octacoordinate analogs. This decrease in coordination number from nine to eight is observed due to lanthanide contraction of thulium [52]. An X-ray diffraction study of a single crystal revealed a *C2/c* crystallographic space group. Moieties of the $[Tm(DOTA)]^-$ are bridged by a potassium ion through three carboxylate groups of three different thulium-DOTA complex units as shown in the packing structure in Fig. 12. Elongation of the nitrogen atoms from Tm(III) metal center (Tm–N ~ 2.53 Å) are noticeably shorter by > 0.08 Å compared to other nine-coordinate DOTA systems. The Tm–O bond lengths remain within the acceptable range (Tm–O ~ 2.279 Å). Significant noticeable differences observed for this particular complex are the widening of N–Tm–N angles both for *cis* (~70.35°) and *trans* (~109.11°) and narrowing of O-Tm-O angles (*cis* ~77.42°, *trans* ~124.34°). These deviations are also observed for other eight coordinate DOTA systems (e.g. Bi(III) and Ca(III)).

3.2.6. Holmium: Na[Ho(DOTA)(H_2O)]·4H_2O

Benetollo et al. described the holmium(III) coordinated DOTA complex in 1999. It showed a structure isomorphous to most enneacoordinate DOTA analogs. This system has a *Pī* crystallographic space group and a triclinic crystal system. The Ho(III) atom is coordinated to the N-donors with a mean distance of 2.64 Å. The four oxygen atoms of the carboxylate groups are bound to Ho(III) are relatively shorter by 0.31 Å when compared to the Ho–N elongation. The distance of the water molecule from the metal center (Ho–Ow1) is ~2.44 Å. Ho(III) is positioned in between the N_4 and O_4 planes by a distance of 1.608 Å and 0.727 Å respectively.

3.2.7. Dysprosium: Na[Dy(DOTA)(H_2O)]·Na(OH)·7H_2O

In the dysprosium complex of DOTA, the single crystal was determined via Patterson and Fourier methods to have the crystallographic space group *P2/c* with a monoclinic crystal system. The molecular structure of Na[Dy(DOTA)(H_2O)]·Na(OH)·7H_2O reveals that all the nitrogen atoms and oxygen atoms are coordinated to the metal center completely encaging the Dy(III) atom. A water molecule additionally binds to Dy(III) completing the nine-coordinate square antiprism geometry. All bonds formed by Dy(III) with nitrogen donors (2.62 Å) and oxygen donor sets (2.34 Å) fall within the range of bond distances observed for this class. Each asymmetric unit of the Dy(III) macrocycle is interestingly linked to another unit forming polymeric chains by two sodium atoms as shown in Fig. 13. The sodium atoms link four units of the Dy(III)–DOTA analog via edge-sharing of the carboxyl functional groups of the polyaminocarboxylate ligand. The sodium atoms are uniquely connected to each other via a bridging hydroxide group (O1A). It is worth noting that the sodium atoms are surrounded by different oxygen donor groups. For a more detailed description, please review literature published by Benetollo et al. [52].

3.2.8. Lutetium: Na[Lu(DOTA)(H_2O)]·4H_2O

Similar to the other nine-coordinate DOTA derivatives, the lutetium analog crystallizes as Na[Lu(DOTA)(H_2O)]·4H_2O in the triclinic unit cell with the space group *Pī*. Again, the molecular

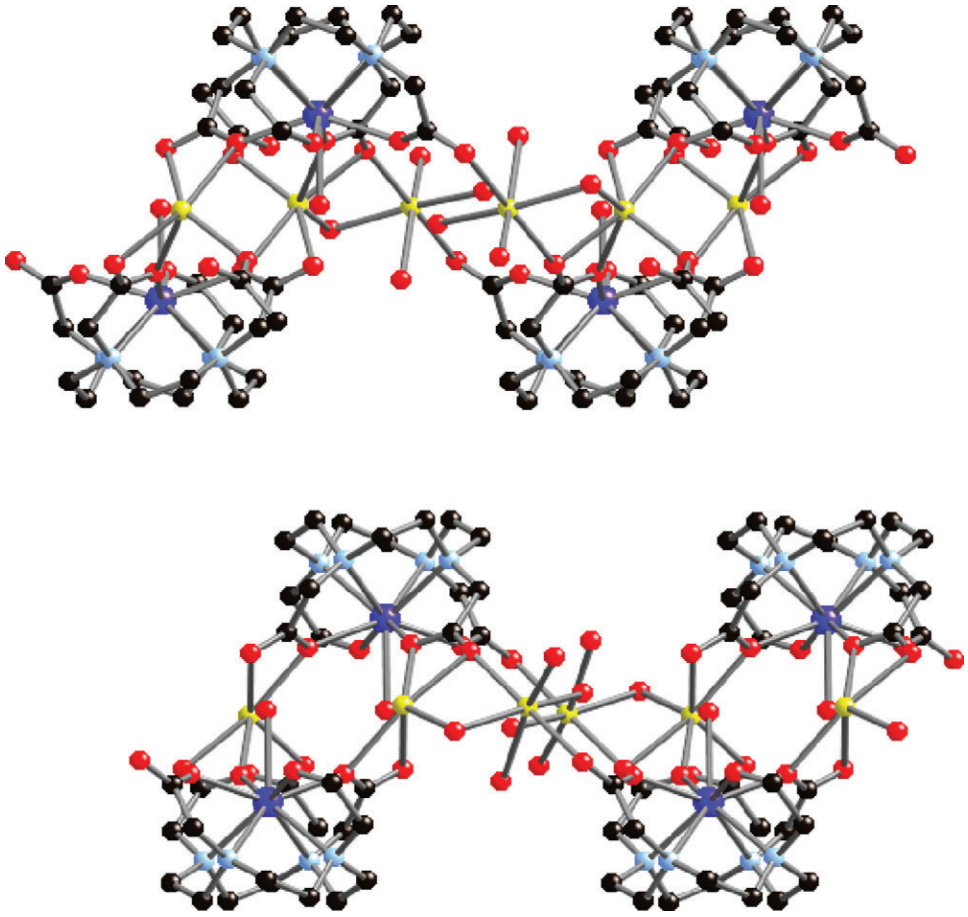


Fig. 13. The packing diagram of Na[Dy(DOTA)(H_2O)]·Na(OH)·7H_2O through the *y*-axis.

Fusion Pharmaceuticals, Inc.
Exhibit 1035.011

structure of this system involves all four nitrogen atoms and four oxygen atoms coordinated to Lu(III) with an oxygen donor from water which acts as the capping ligand. The N_4 and O_4 donor sets form a plane separately acting as square bases at the top and bottom of the Lu(III) atom. The twist angle of the two planes is 39°. The N_4 plane is separated from the Lu(III) metal center by 1.586 Å. The distance of the Lu–O_4 plane is measured as ~0.732 Å. Elongation of Lu–N bonds has a mean length of 2.614 Å, considerably longer than Lu–O (2.279 Å) by 0.335 Å.

3.2.9. Neodymium: $Na[Nd(DOTA)(H_2O)]\cdot 4H_2O$

In the crystal structure of $Na[Nd(DOTA)(H_2O)]\cdot 4H_2O$, the macrocylic ligand DOTA encapsulates the Nd(III) atom to form a square antiprismatic structure isostructural to the geometry of $Na[Pr(DOTA)(H_2O)]\cdot 4H_2O$ [52]. The mean Nd–N distance is determined to be ~2.70 Å. The Nd(III) center is bound to hydroxyl groups of the four carboxylate arms with a shorter distance (Nd–O ~ 2.42 Å) compared to the N-donors. Water occupies the ninth coordination site of the Nd-DOTA complex (Nd–Ow ~ 2.508 Å). The molecular unit of this complex is shown to form a one-dimensional polymeric chain. The polymer chain is formed by a bridging sodium atom bound to the oxygen atoms of the carboxylate arms of three DOTA (see Fig. 14 for packing).

3.2.10. Praseodymium: $Na[Pr(DOTA)(H_2O)]\cdot 4H_2O$

Crystals of the molecular structure of $Na[Pr(DOTA)(H_2O)]\cdot 4H_2O$ were determined to possess square antiprismatic structures [52]. The coordination around Pr(III) involves all N- and O-donor atoms of the DOTA ligand with a monocapped aquo ligand forming a nine-coordinate geometry. With the O and N donor atoms, the mean M–L bond distances are 2.46 Å (O) and 2.721 Å (N) respectively. The Pr(III) atom is displaced from the N_4- and O_4-planes by a distance of 1.695 Å and 0.671 Å respectively.

3.2.11. Cerium: $Na[Ce(DOTA)(H_2O)]\cdot NaHCO_3\cdot 7H_2O$

Crystals of the DOTA complex of Ce(III) occurred via acetone vapor diffusion into the water solution of the reaction. The structure of $[Ce(DOTA)(H_2O)]^-$ possesses the crystallographic space group $P2_1$ with a monoclinic system [52]. Coordination around the Ce(III) atom involves the N4 and O4 donor set. Its geometry is a twisted square antiprism with a twist angle of 25° formed by the N-plane and O-planes. The Ce–N bond distances range from 2.69–2.77 Å while the Ce–O bonds elongate with a mean length of 2.46 Å. The distance between Ce and Ow1 from the capping water ligand is measured approximately ~2.598 Å. Aside from $[Ce(DOTA)(H_2O)]^-$, the asymmetric unit cell involves six water molecules coordinated to sodium ion (Na1) and a sodium (Na2) bicarbonate with one

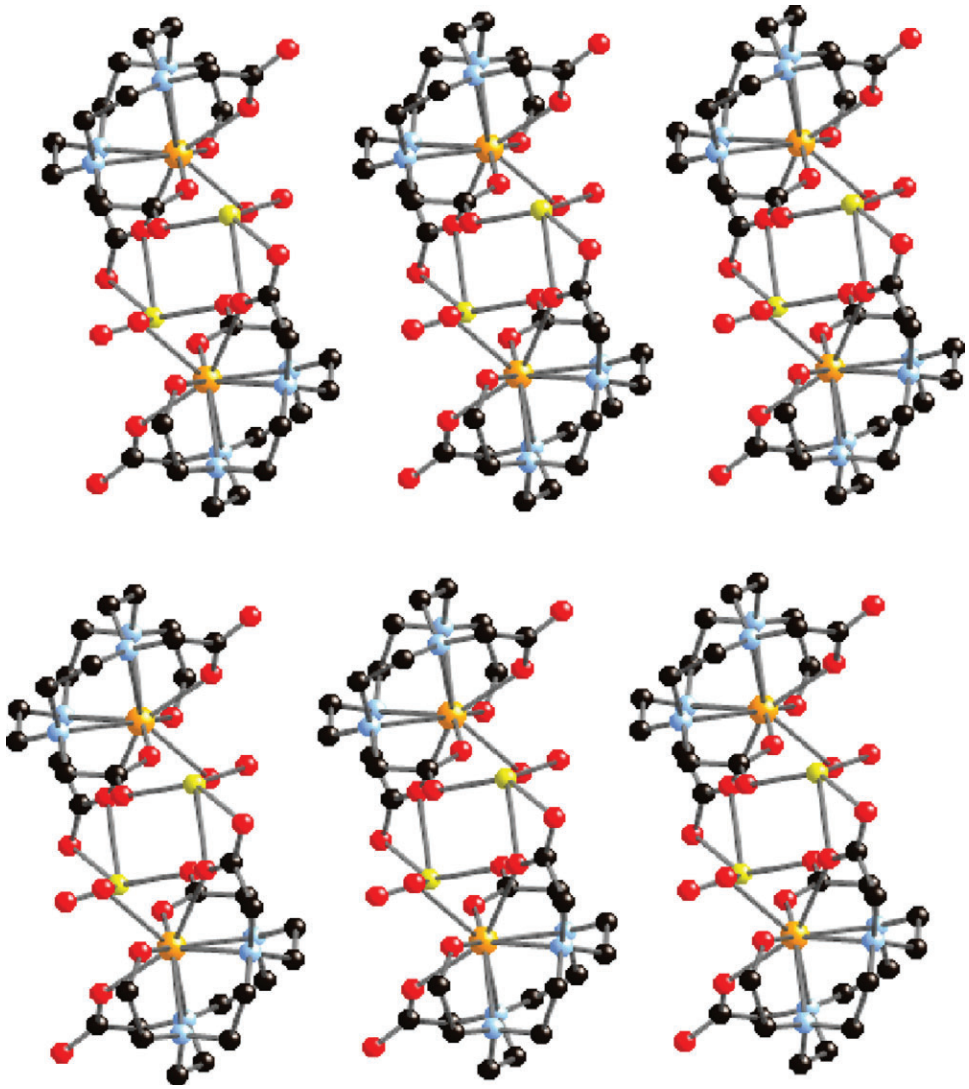


Fig. 14. One-dimensional polymeric diagram of $Na[Nd(DOTA)(H_2O)]\cdot 4H_2O$ shows bridging through sodium atoms as viewed along the *y*-axis. This packing motif is similar across most lanthanide structures having the same molecular geometry.

Fusion Pharmaceuticals, Inc.
Exhibit 1035.012

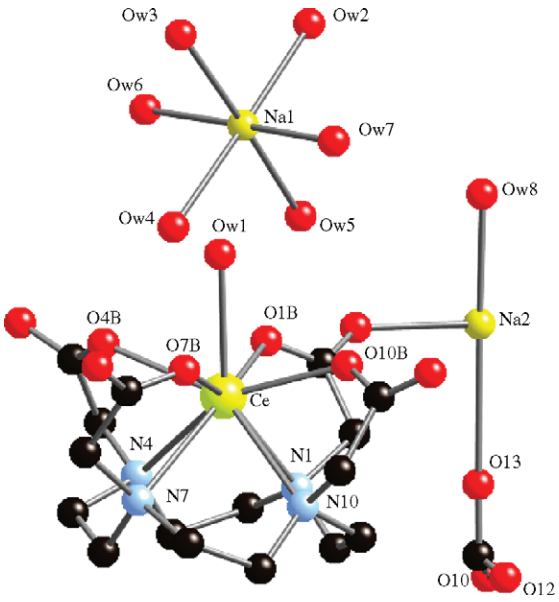


Fig. 15. The molecular structure of $Na[Ce(DOTA)(H_2O)]\cdot NaHCO_3\cdot 7H_2O$ viewed through the *x*-axis. Two sodium atoms, one coordinated and the other present as the hydrogen carbonate salt, are also shown. Hydrogen atoms and lattice waters are omitted for clarity.

molecule of water coordinated to the sodium cation as shown in Figs. 15 and 16.

The Ce(III) atom is displaced from the N_4 and O_4 plane by a distance of 1.765 Å and 0.604 Å, respectively. Acute angles formed by N–Ce–N measure an average of 65.34° and for nitrogen atoms *trans* to each other angles of 98.92 ° and 100.13° are formed. Angles formed by *cis* O–Ce–O are wider compared to those angles formed by the N-donor atoms with 83.7°, 84.57°, 84.98° and 85.14°. Consequently, *trans* O–Ce–O angles are determined to have a mean angle of 144.26°.

3.2.12. Lanthanum: $Na[La(HDOTA)La(DOTA)]\cdot 10H_2O$

$Na[La(HDOTA)La(DOTA)]\cdot 10H_2O$ is an inverted square antiprism with a $P2_1/n$ space group [62]. The molecular structure of this white crystal is unique in its coordination because it is dimerized via a direct interaction with another unit. The carbonyl oxygen of the carboxylic arm bridges two molecular units by coordinating to the metal center forming a nine-coordinate geometry(see Fig. 17). All bond lengths and angles are consistent with the ranges observed for lanthanide systems. The twist angles for both units are ~21° and 23°. This places the crystal intermediate between a prismatic and antiprismatic structure with ideal twist angles of 0° and 45° respectively.

3.2.13. Calcium: $Ca(OH_2)_3[CaDOTA]\cdot 7.7H_2O$

The molecular structure of this derivative is octacoordinate with a space group of *C2/c* having a distorted square antiprismatic geometry with $Z = 8$. The packing scheme is shown in Fig. 18. Calcium is bound to the four nitrogen atoms of the ring with a mean distance of 2.591 Å [53]. It is further encapsulated by all four oxygen atoms from the carboxyl group with the mean length of 2.418 Å. N–Ca–N bond angles formed has an average of 69.56°. The largest N–Ca–N bond angles are measured to be on average at 107.33°. The angles formed by the carboxyl oxygen atoms are wider at 78.25° and 126.37°. Ca(II) is puckered from the N_4 plane by a distance of 1.549 Å and displaced from the O_4 plane by 1.095 Å.

3.2.14. Strontium: $\{(C(NH_2)_3)_2[Sr(DOTA)(H_2O)]\}\cdot 4H_2O$

$[Sr(DOTA)(H_2O)]^{2-}$ is a nine-coordinate twisted square antiprism. The ligand has all four nitrogen atoms of the cyclen ring and oxygen atoms of the carboxyl arms bound to the metal. Water caps the coordination sphere [61]. Strontium(II) is bound to the four nitrogen atoms of the polyazamacrocycle by an equidistance of 2.732 Å and to the oxygen atoms by equivalent bond lengths of 2.548 Å. The ninth coordinated oxygen from the water ligand is 2.849 Å from the metal center. The angles formed by N–Sr–N and O–Sr – O are identical at 66.19° and 71.33° respectively. The metal is displaced from the N_4-plane by 1.736 Å and from the O_4-plane by 0.816 Å.

3.2.15. Scandium: $3(Na[Sc(DOTA)])\cdot NaOH\cdot 18H_2O$

The molecular structure of $3(Na[Sc(DOTA)])\cdot NaOH\cdot 18H_2O$ is characterized by Bombieri et al. [52]. The single crystal of $[Sc(DOTA)]^-$ reveals an octacoordinate square prismatic geometry (see Fig. 19a and b). Two of the units (of three in the unit cell) are linked by octahedral sodium atoms bound to carboxylate oxygen atoms of the macrocycle and of water molecules. The other $[Sc(DOTA)]^-$ unit is connected to the other moieties through hydrogen bonds formed with water molecules. Remarkably, the bond lengths of all Sc–N (~2.445 Å) bonds as well as the Sc–O bonds

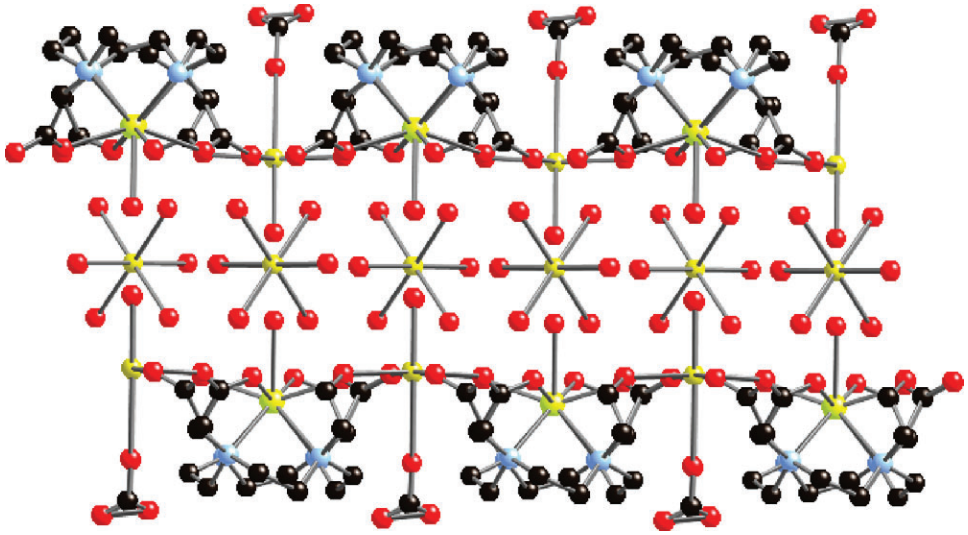


Fig. 16. The packing diagram of the cerium analog of DOTA along the *y*-axis.

Fusion Pharmaceuticals, Inc.
Exhibit 1035.013

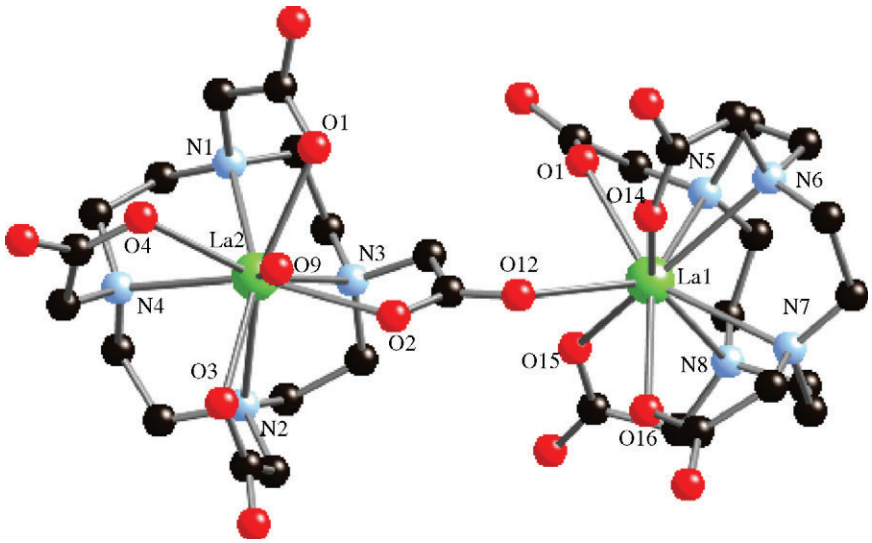


Fig. 17. Looking down the *z*-axis, the units of $[La(DOTA)]^-$ are directly coordinated via a bridge formed through a carbonyl oxygen of one of the carboxylic acid functional groups.

(~2.154 Å) are symmetrical. These shorter elongations make this structure uniquely compact compared to other square antiprismatic DOTA analogs [52].

4. Solid state structure in correlation to stability

Correlation of the observed stabilities, log K_d (defined as dissociation constant), to the solid-state structures of the metal–DOTA complexes is not as straightforward as it may seem. As a result of the complexes' differences in geometry, ionic size and inherent properties, various perspectives as to observed trends are presented. Different bond lengths and angles as well as displacements from the nitrogen and oxygen planes, dihedral angles or twist angles where appropriate were determined and analyzed. Tables 4 and 5 lists stability constants as well as mean bond lengths, angles and plane displacements of 6–9 coordinate metal–DOTA systems.

From Table 4, the order of stability for complexes with known log K_d values appears: Fe(III) > Cu(II) > Ga(III) > Ni(II) > Co(II) > Zn(II). It is apparent that Fe(III) has the highest stability because of the three carboxylate arms bonded to the metal center. The Fe–N mean distance is longer than Fe–O bond length. Fe(III) being a hard acid is attracted more towards oxygen donors. The presence of an additional arm locks in the Fe(III) in the cage hence, any nucleophilic attack is prevented. In contrast, six-coordinate DOTA complexes have lower stability. The Cu(II) DOTA complex appears to have Jahn-Teller distortion of its octahedron with four short bonds in the equatorial planes and two long bonds at the axial positions. A closer look at the bond distances of the metal and the electron donors occupying the equatorial sites of the ligand shows that the distances are smaller in comparison to bond lengths at the same positions with Ga(III), Ni(II), Co(II) and Zn(II). Electrostatic interactions between Cu(II) and the N- and O-donors are stronger keeping the metal chelated. This increases the thermodynamic stability of Cu(II) against the other three metal systems. This stability is confirmed by the Irving–Williams order of transition metal complex stabilities for divalent species in the following sequence: Cu(II) > Ni(II) > Co(II) > Fe(II) > Mn(II) [68]. Co(II) is less stable than Ga(III) because the M–N bond distances for Co(II) are slightly longer than Ga(III). Ga(III) is also more electropositive than the former metal ion. The DOTA complex of Zn(II) is the least stable among the six-coordinate metal–DOTA systems due to its filled d^{10}shell. Having a d^{10} electron configuration prevents Zn(II) from easily accepting charge transfers from N and O-donors. Although it can very well form covalent compounds with N-donor ligands, due to its lesser degree of polarization and a lack of crystal field stabilization as a consequence of its filled shell, Zn(II) highly favors four-coordinate tetrahedral complexes. The distortion in the octahedron of this crystal structure is evident in the asymmetrical bond

Table 4
List of stability constants, observed bond lengths, angles and plane displacements of metal–DOTA complexes having 6–7 coordination numbers.

Metal ion	Stability constant, log K_d	M–N_{eq} average bond length, Å	M–O	N_4–plane distance, Å
Fe(III)	29.40[a] 24.48[b]	2.280	2.05	1.058
Cu(II)	22.72[c] 22.25[a]	2.107	1.966	0.916
Ga(III)	21.33[a]	2.112	1.934	0.840
Ni(II)	20.50[c] 20.03[b]	2.113	2.025	0.821
Co(II)	19.30[c] 20.27[b]	2.166	2.034	0.888
Zn(II)	18.70[c] 21.099[b]	2.171	2.037	0.891

[a] Ref. [69].
[b] Ref. [70].
[c] Ref. [71].

Fusion Pharmaceuticals, Inc.
Exhibit 1035.014

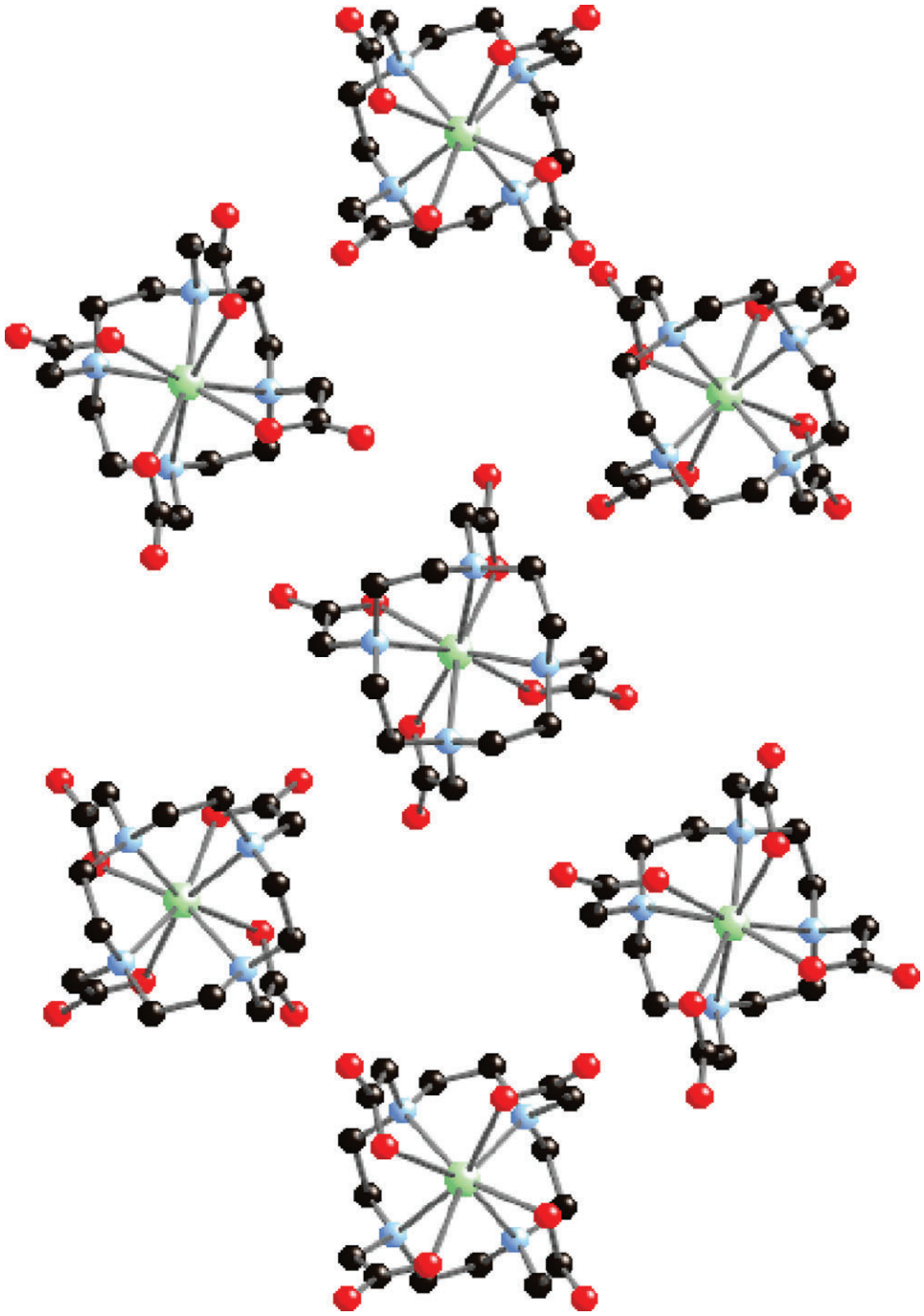


Fig. 18. The packing system of $Ca(OH_2)_3[CaDOTA]\cdot 7.7H_2O$ as viewed along the *y*-axis is a polymeric structure bridged by discrete calcium atoms bound to the carboxyl oxygen atoms of the monomeric units.

distances of the N and O-donor groups. From Table 2, two M–N bonds at the axial positions are longer than the M–N bonds found at the equatorial positions. The two oxygen atoms occupying the other two equatorial sites are even shorter in length compared to the nitrogen atoms in the same equatorial plane.

For the metal–DOTA complexes with coordination number 8 or 9, the order of increasing stability then is as follows: Bi(III) > Lu(III) > Dy(III) > Gd(III), Ho(III), Tm(III), Sc(III), Y(III) > Eu(III) > Ce(III) > Nd(III), Pr(III) > La(III) > Ca(II) > Sr(II) (see Table 5). Several factors affect the stability of metal–DOTA complexes with 8–9 coordination states. An acidic pH catalyzes dissociation of the metal complex because it prompts protonation of the carboxylate and amino functional groups of the cyclen [72,73]. The degree of distortion of the twist or dihedral angles of the square prism and displacement of the metal from the nitrogen plane directly influence the encapsulation of the metal by the ligand [54].

Of all metal–DOTA structures, Bi(III) appears as the most stable with a stability constant of log K_d ~30.3. The mean bond distance between the coordinating nitrogen atoms and oxygen atoms are almost equidistant at 2.5 Å with a difference of 0.012 Å. The Bi(III)–N average bond lengths are relatively shorter causing deeper encapsulation of the metal in the macrocyclic cage. Fig. 20 displays the trend observed across metals with decreasing thermodynamic

Fusion Pharmaceuticals, Inc.
Exhibit 1035.015

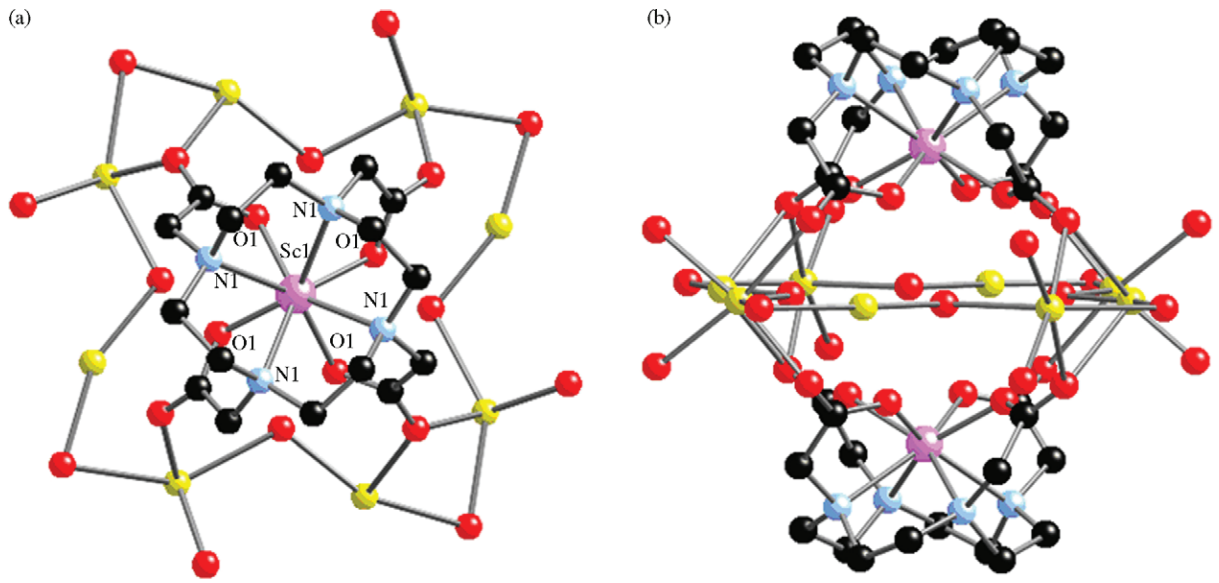


Fig. 19. (a) The molecular structure of 3(Na[Sc(DOTA)])·NaOH·18H_2O viewed along the crystallographic *z*-axis; (b) From the crystallographic *x*-axis, an intricate network of sodium atoms is seen bound to the lattice waters and carboxyl oxygen atoms bridge two units of $[Sc(DOTA)]^-$.

Table 5
List of stability constants, observed bond lengths, bond angles and plane displacements of metal–DOTA complexes having coordination numbers 8 or 9.

Metal ion	Stability constant, log *K*	M–N average bond length, Å	M–O average bond lengths, Å	M–Ow* distance, Å	N–plane distance, Å	O_4-plane distance	Twist angles	Isomer type
Bi(III)	30.3[a]	2.526	2.538	n/a	1.434	1.112	39	SA'
Y(III)	24.3[e] 24.4[f]	2.646	2.323	2.435	1.616	0.718	40	SA
Gd(III)	24.0[b] 22.1[d] 23.6[g] 24.7[h]	2.663	2.368	2.463	1.632	0.715	38.5	SA
Eu(III)	23.7[g] 26.21[i] 28.2[j] 23.5[h]	2.676	2.379	2.484	1.645	0.71	39	SA
Tm(III)	23.7[g] 24.4[h]	2.279	2.529	n/a	1.466	1.064	25	TSA'
Ho(III)	23.5[g] 24.5[f] 24.5[h]	2.641	2.330	2.443	1.608	0.727	39	SA
Dy(III)	23.5[g] 23.93[k] 24.8[h]	2.623	2.338	2.479	1.585	0.755	38	SA
Lu(III)	23.5[g] 23.06[k] 29.2[j] 25.4[h]	2.614	2.279	2.416	1.586	0.732	39	SA
Nd(III)	22.5[g] 23.0[h]	2.703	2.416	2.508	1.676	0.684	39	SA
Pr(III)	22.4[g] 23.0[h]	2.721	2.431	2.53	1.695	0.671	39	SA
Ce(III)	21.6[g] 24.6[l] 23.4[h]	2.733	2.460	2.598	1.765	0.604	25	TSA
La(III)	21.6[b] 20.7[g] 22.9[h]	2.782	2.493	2.554	1.822	0.715	21, 23	TSA
Ca(II)	16.37[c]	2.591	2.418	n/a	1.549	1.095	22.5	TSA'
Sr(III)	14.38[c]	2.732	2.548	2.849	1.736	0.816	23.9	TSA
Sc(III)	24.2[m]	2.444	2.147	n.a.	1.327	1.007	41.16, 40.15	SA'

*For clarity and convention, M–Ow refers to the bond formed by the metal and an oxygen from a different ligand species. [a]Ref. [54]; [b]Ref. [69], [c]Ref. [71]; [d]Ref. [72]; [e]Ref. [74]; [f]Ref. [75]; [g]Ref. [76]; [h]Ref. [77]; [i]Ref. [78]; [j]Ref. [79]; [k]Ref. [80]; [l]Ref. [81]; [m]Ref. [82].

Fusion Pharmaceuticals, Inc.
Exhibit 1035.016

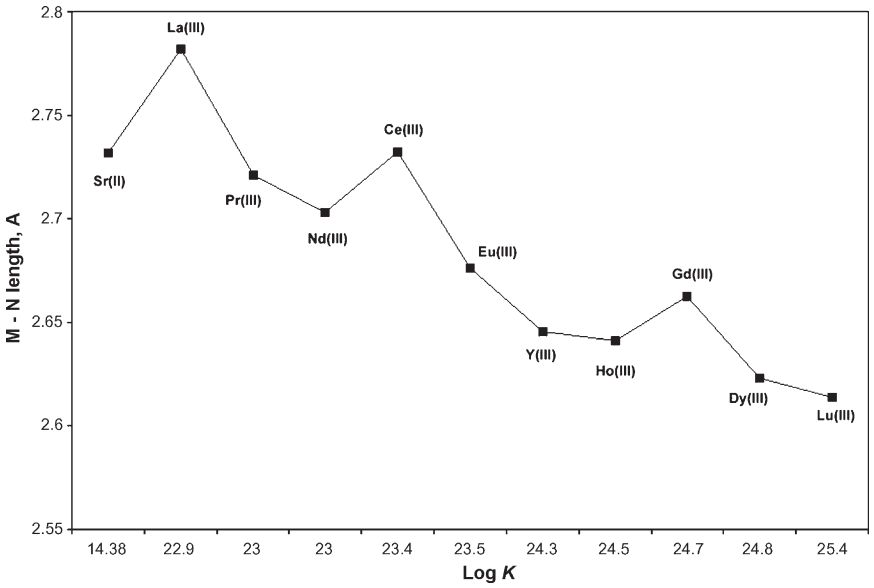


Fig. 20. Plot of M–N bond distances vs. stability, log K_d showing a downward trend in bond lengths with increasing stability. Stability constants are based on Refs. [54,74,77] since the log K_d constants were measured under similar conditions (e.g. same temperature).

stability versus mean M–N distance for nine-coordinate DOTA complexes.

With the exception of Bi(III), Sc(III), Tm(III) and Ca(II), the rest of the metal–DOTA chelates are observed to have lower stabilities due to the presence of a ninth coordination site. The presence of a ninth coordinating ligand is observed to pull the metal from the amine cage. This occurrence is consistent with the observed increase in the measured distance from the metal to the N_4 plane. Dissociation through acid catalysts [73] can then readily occur. In addition, shorter distances between the capping water molecule from the metal center places the aquo ligand in a sterically hindered position and the less likely it will be able to conduct hydrogen bonding which would allow protonation of the donor atoms [47]. This is consistent with the observed trend upon plotting the stability constants vs. M–Ow distances for each enneacoordinate structure as shown in Fig. 21. It is to be expected that due to lanthanide contraction (increasing effective charge and reduced ionic radius) that the structure of the DOTA complexes would become more compact and the metal bound water would be 'pushed' away. This would then be reflected by a lengthening of the bound water-metal distance and so an increasing water exchange rate going from La(III) to Lu(III). The caveat however for this section is that we are attempting to correlate solid-state structures with stability measured in solution. The two do not necessarily allow for such fitting but it is interesting to us none-the-less to follow fit versus intuitive expectations. Based on ionic size alone, Lu(III) (0.861 Å) should be a significantly thermodynamically stable DOTA complex. From the plot in Fig. 21, Lu(III) noticeably has the shortest metal–Ow distance next to Bi(III). The water ligand is bound tightly in the crystal lattice. Lu(III) is displaced from the N_4-plane by 1.586 Å which is more than twice the length of its distance from the O_4-plane. These observed bond lengths are consistent with the observed stability trend for Lu(III). From Table 5, Dy(III) has a slightly higher M–Ow elongation compared to Gd(III), Ho(III), Sc(III) and Y(III). This lanthanide, however, is more tightly encapsulated in the cavity of the macrocyle as demonstrated by shorter M–N lengths (~2.623 Å) and N–plane distance (~1.685 Å). Gd(III), Y(III) and Ho(III) crystallized in the same space group $P\bar{1}$. Their stabilities vary by ±0.3 units. The M–N bond lengths, M–Ow elongations and the distances of the metal to the N_4-plane are within close range of each other. It can then be assumed that their stabilities are more or less equivalent. On the other hand, Sc(III), a d^1 transition metal, possesses a trivalent oxidation state making it more electropositive. Hence, metal-ligand electrostatic and covalent bonding interactions are stronger. The absence of water or a ninth coordinating ligand at the apex of the square antiprism prevents the metal from being pulled out of the macrocyclic cage. A closer look at its crystal structure reveals a compact coordination sphere with the mean Sc–N (~2.444 Å) and Sc–O (~2.147 Å) bond lengths significantly shorter overall. With Tm(III), the lack of an aquo ligand can effect a more compact packing of its crystal structure, effecting a greater stability among heavier lanthanides further up the series (i.e. La(III), Ce(III), Pr(III), Nd(III), Eu(III)). Its displacement from the N_4-plane by 1.466 Å is relatively shorter than other lanthanide displacements. Thus, stronger electron interactions can occur between the polycyclic amines and Tm(III). The ionic radius of Tm(III) is also smaller than its predecessors in the series due to lanthanide contraction [67]. The rest of the other lanthanide–DOTA chelates have decreasing stabilities based on M–Ow bond lengths. The lanthanum derivative is bound to another molecular unit via carbonyl oxygen that occupies the ninth coordination site. The M–O bond distance (~2.553 Å) for this analog is consistent with the observed trend for decreasing stability.

While lanthanides and alkaline earth metals form strongly ionic bonds, lanthanides are found to have some degree of covalency, reinforcing electrostatic ligand interactions compared to purely electrostatic interactions found with alkaline earth metals [83]. Hence, Ca(II) and Sr(II) are the least stable of the DOTA systems at log $K_d \sim 16.37$ and 14.38 respectively. These alkaline earth metals are highly ionic in character. There is a tendency then to form salts with electronegative anions rather than covalently bind to available N and/or O-donors. In terms of structure, Sr(II) is the least stable thermodynamically because of its size and ionic charge. According to Fajans' rules, cations having a low positive charge and a large ionic size tend to form ionic bonds [68]. Furthermore, bonds formed between two atoms with a large electronegativity difference are ionic in nature. These characteristics fit Ca(II) and Sr(II). The electronegativity difference between Ca and O is ~2.44 and with N is ~2.04 [67]. The electronegativity of Sr, on the other hand, differs from O by 2.39 and from N by 1.99 [67]. Ca(II) and Sr(II) have bigger ionic sizes compared to the other cations and a lower oxidation state (+2) with an empty *s* valence shell. Hence, these cations will generally favor ionic bonds with anions rather than

Fusion Pharmaceuticals, Inc.
Exhibit 1035.017

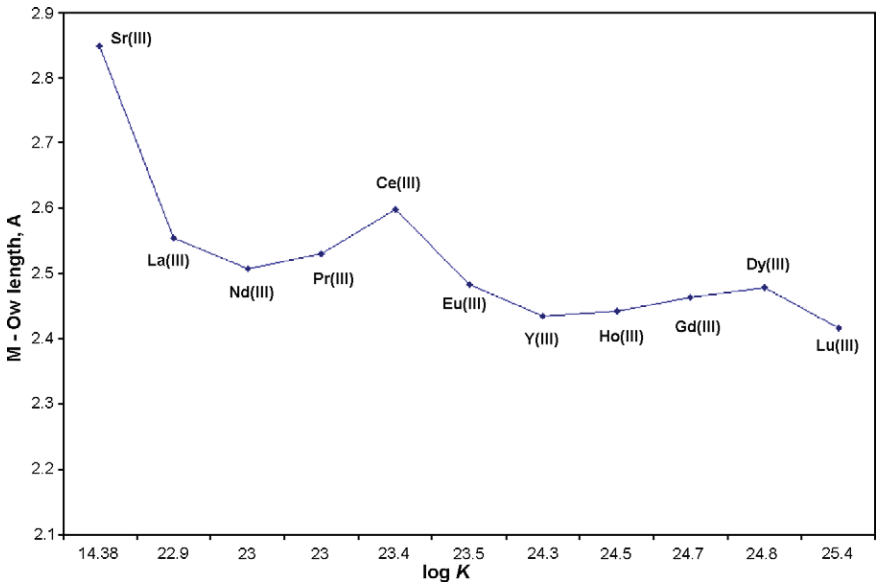


Fig. 21. The plot of M–Ow against stability, log K_d. Based on the trend observed, M–Ow bond distances are indirectly proportional to stability. Stability constants are based on Refs. [54,74,77] to ensure that log K_d constants are measured under similar conditions.

form covalent bonds through *sp* hybridization. Indeed, the nature of bonding in lanthanide and alkali earth metal DOTA complexes is predominantly ionic with very little covalency. Structurally, the lack of water in its unit cell provided Ca(II) more stability than Sr(II). Although Ce(II) has roughly equivalent M–N bond distances, Sr(II) has a greater displacement from the N-plane. From the observed M–Ow bond length, Sr(II) has the greatest bond distance from water which is indirectly proportional to stability.

The solid phase structures of these metal–DOTA complexes do not always reflect their structures in solution. Desreux, in 1980, reported the existence of two square enantiomers of lanthanide-DOTA complexes via nuclear magnetic resonance studies [84]. Since then extensive studies have been conducted to confirm the identity of these two isomers of the LnDOTA complex in solution: square antiprismatic (SA) and twisted square antiprismatic (TSA) geometry (see Fig. 21) [52,85,86]. In solution, the complex are seen to possess variations involving rotation of the acetate side arms as well as the ethylene moieties [52,85]. SA DOTA structures are shown to possess twist angles of ∼39°, a minor deviation from the ideal twist angle value of 45°. Smaller twist angles are observed for TSA isomers in general (∼22°–23°) [58]. A comparison of the cavities of the TSA and SA geometries reveal that SA structures have smaller, more compact cages than TSA [52]. The different LnDOTA complexes are categorized in Table 5 under the two different enantiomers with SA' and TSA' listed as subcategories with no ninth coordinating ligand. These subcategories are even more compact than their counterparts due to the lack of an apical coordinating ligand [52]. Ratios of these isomers in solution are very difficult to elucidate with no specific trend observed [86]. Comparisons of the solution structures of the DOTA complexes of La(III) and Lu(III) via NMR revealed similarities in their structures. These investigations observed an inversion of stabilities at the opposite ends of the lanthanide series [62,86]. From these observations, there appears to be conformity in the stability trends between solution phase geometries and solid phase structures of metal–DOTA complexes (Fig. 22).

5. Summary

This review puts forward different coordination geometries of twenty-two coordinated DOTA systems. Analysis of the different crystal structures and correlating trends in bond lengths, angles and plane distances are not straightforward. However, we have categorized the crystal structures into two classifications in order to provide a thorough and clear-cut comparison of crystallographic data. Class A metal–DOTA systems include six to seven coordinate derivatives while Class B molecular struc-

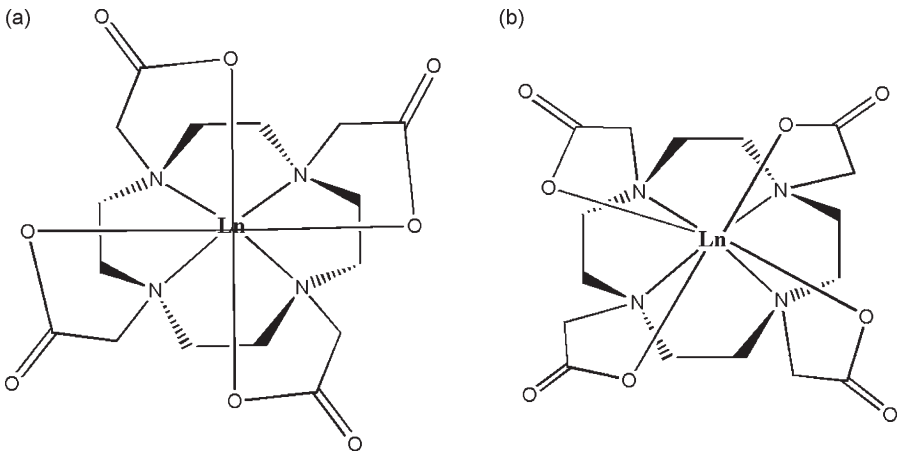


Fig. 22. Schematic illustration of LnDOTA isomers: (a) square antiprismatic and (b) twisted square antiprismatic geometries.

Fusion Pharmaceuticals, Inc.
Exhibit 1035.018

tures have coordination numbers seven to eight. For Class A, thermodynamic stability increases in the following sequence: Fe(III) > Cu(II) > Ga(III) > Ni(II) > Co(II) > Zn(II). A higher coordination state leads to an increase in stability due to better accommodation of the ligand's electron density. The bond lengths between the metal and the amine cage are also indicative of stability with a shorter M–N distance providing increased interaction between the metal and electron donor. Hence, greater stability is achieved. Class B coordinates do not behave similarly to the previous lower coordination group with the following sequence of increasing stabilities: Bi(III) > Lu(III) > Dy(III) > Gd(III), Ho(III), Tm(III), Sc(III), Y(III) > Eu(III) > Ce(III) > Nd(III), Pr(III) > La(III) > Ca(II) > Sr(II). The presence of water as the ninth capping ligand decreases the stability of the metal complex. The plot of M–Ow bond length and stability clearly reveals an indirectly proportional relationship with a lowering of log *K* upon an increase of M–Ow bond distances. M–N bond distances also play a role in determining stability. With shorter M–N bond distances, the metal cation is better encapsulated by the macrocycle thus limiting decomplexation. In addition, the inherent properties of the metals (i.e. ionic size, electronegativity) must also be considered to explain variability in the trends observed. Taking all these factors in consideration the solid-state structure can offer significant insight into complex stability.

Acknowledgements

The authors would like to thank Oluwatayo F. Ikotun and Dr. Wayne Ouellette (Dept. of Chemistry, Syracuse University) and Tracy Allgood (CCDC) for their assistance in preparing this manuscript. We also thank numerous authors who provided us with original crystal files upon request.

References

[1] M.R. Spirlet, J. Rebizant, J.F. Desreux, M.F. Loncin, Inorg. Chem. 23 (1984) 359.
[2] A. Riesen, M. Zehnder, T.A. Kaden, Helvetica Chim. Acta 69 (1986) 2067.
[3] M. Magerstadt, O.A. Gansow, M.W. Brechbiel, D. Colcher, L. Baltzer, R.H. Knop, M.E. Girton, M. Naegele, Magn. Reson Med. 3 (1986) 808.
[4] N.A. Viola, R.S. Rarig, W. Ouellette, R.P. Doyle, Polyhedron 25 (2006) 3457.
[5] M. Woods, A.D. Sherry, Inorg. Chem. 42 (2003) 4401.
[6] S. Zhang, R. Trokowski, A.D. Sherry, J. Am. Chem. Soc. 125 (2003) 15288.
[7] C. Adair, M. Woods, P. Zhao, A. Pasha, P.M. Winter, G.M. Lanza, P. Athey, A.D. Sherry, G.E. Kiefer, Contrast Media Mol. Imaging 2 (2007) 55.
[8] J. Vipond, M. Woods, P. Zhao, G. Tircso, J. Ren, S.G. Bott, D. Ogrin, G.E. Kiefer, Z. Kovacs, A.D. Sherry, Inorg. Chem. 46 (2007) 2584.
[9] B. Yoo, M.D. Pagel, Bioconjug. Chem. 18 (2007) 903.
[10] S. Zhang, M. Merritt, D.E. Woessner, R.E. Lenkinski, A.D. Sherry, Acc. Chem. Res. 36 (2003) 783.
[11] T. Chauvin, P. Durand, M. Bernier, H. Meudal, B.-T. Doan, F. Noury, B. Badet, J.-C. Beloeil, E. Toth, Angewandte Chemie Int. Ed. 47 (2008) 4370.
[12] B. Yoo, M.D. Pagel, J. Am. Chem. Soc. 128 (2006) 14032.
[13] C. van Montfrans, R.J. Bennink, K. de Bruin, W. de Jonge, H.J. Verberne, F.J.W. ten Kate, S.J.H. van Deventer, A.A. te Velde, J. Nucl. Med. 45 (2004) 1759.
[14] C.F. Meares, M.K. Moi, H. Diril, D.L. Kukis, M.J. McCall, S.V. Deshpande, S.J. DeNardo, D. Snook, A.A. Epenetos, Br J. Cancer Suppl. 10 (1990) 21.
[15] W.C. Cole, S.J. Denardo, C.F. Meares, M.J. McCall, D. GL, A.L. Epstein, H.A. O'Brien, M.K. Moi, J. Nucl. Med. 28 (1987) 83.
[16] J. DeNardo Sally, L. DeNardo Gerald, A. Yuan, M. Richman Carol, T. O'Donnell Robert, N. Lara Primo, L. Kukis David, A. Natarajan, R. Lamborn Kathleen, F. Jacobs, L.H. Siantar Christine, Clin. Cancer Res. 9 (2003) 3938S.
[17] S.V. Deshpande, S.J. DeNardo, D.L. Kukis, M.K. Moi, M.J. McCall, D. GL, C.F. Meares, J. Nucl. Med. 31 (1990) 473.
[18] M. Eiblmaier, A. Meyer Laura, J. Anderson Carolyn, J. Cancer Biol. Ther. (2008) 63.
[19] V. Hird, M. Verhoeyen, R.A. Badley, D. Price, D. Snook, C. Kosmas, C. Gooden, A. Bamias, C. Meares, J.P. Lavender, Br. J. Cancer 64 (1991) 911.
[20] R.P. Junghans, D. Dobbs, M.W. Brechbiel, S. Mirzadeh, A.A. Raubitschek, O.A. Gansow, T.A. Waldmann, Cancer Res. 53 (1993) 5683.
[21] M.R. Lewis, J.E. Shively, Bioconjug. Chem. 9 (1998) 72.
[22] M. Li, C.F. Meares, Bioconjug. Chem. 4 (1993) 275.
[23] M. Li, C.F. Meares, Q. Salako, D.L. Kukis, G.-R. Zhong, L. Miers, S.J. DeNardo, Cancer Res. 55 (1995) 5726S.
[24] M.V. Backer, Z. Levashova, V. Patel, B.T. Jehning, K. Claffey, F.G. Blankenberg, J.M. Backer, Nat. Med. (New York, NY, United States) 13 (2007) 504–509.
[25] N. Cauchon, R. Langlois, A. Rousseau Jacques, G. Tessier, J. Cadorette, R. Lecomte, J. Hunting Darel, A. Pavan Roberto, K. Zeisler Stefan, E. van Lier Johan, Eur. J. Nucl. Med. Mol. Imaging 34 (2007) 247.
[26] R. Hsu Andrew, W. Cai, A. Veeravagu, A. Mohamedali Khalid, K. Chen, S. Kim, H. Vogel, C. Hou Lewis, V. Tse, G. Rosenblum Michael, X. Chen, J. Nucl. Med. 48 (2007) 445.
[27] A.M. Wu, P.J. Yazaki, S.w. Tsai, K. Nguyen, A.L. Anderson, D.W. McCarthy, M.J. Welch, J.E. Shively, L.E. Williams, A.A. Raubitschek, J.Y. Wong, T. Toyokuni, M.E. Phelps, S.S. Gambhir, Proc. Natl. Acad. Sci. 97 (2000) 8495.
[28] Y. Wu, X. Zhang, Z. Xiong, Z. Cheng, R. Fisher Darrell, S. Liu, S. Gambhir Sanjiv, X. Chen, J. Nucl. Med. 46 (2005) 1707.
[29] P. Li Wen, S. Lewis Jason, J. Kim, E. Bugaj Joseph, A. Johnson Michael, L. Erion Jack, J. Anderson, J. Bioconjug. Chem. 13 (2002) 721.
[30] M. Van Essen, E.P. Krenning, M. De Jong, R. Valkema, D.J. Kwekkeboom, Acta Oncol. 46 (2007) 723.
[31] M. Van Essen, E.P. Krenning, M. De Jong, R. Valkema, D.J. Kwekkeboom, Acta Oncologica 46 (2007) 723.
[32] M. Henze, A. Dimitrakopoulou-Strauss, S. Milker-Zabel, J. Schuhmacher, L.G. Strauss, J. Doll, H.R. Macke, M. Eisenhut, J. Debus, U. Haberkorn, J. Nucl. Med. 46 (2005) 763.
[33] S. Vallabhajosula, I. Kuji, K.A. Hamacher, S. Konishi, L. Kostakoglu, P.A. Kothari, M.I. Milowski, D.M. Nanus, N.H. Bander, S.J. Goldsmith, J. Nucl. Med. 46 (2005) 634.
[34] M. de Jong, W.H. Bakker, E.P. Krenning, W.A. Breeman, M.E. van der Pluijm, B.F. Bernard, T.J. Visser, E. Jermann, M. Behe, P. Powell, H.R. Macke, Eur. J. Nucl. Med. 24 (1997) 368.
[35] A. Otte, R. Herrmann, A. Heppeler, M. Behe, E. Jermann, P. Powell, H.R. Maecke, J. Muller, Eur. J. Nucl. Med. 26 (1999) 1439.
[36] L. Bodei, D. Handkiewicz-Junak, C. Grana, C. Mazzetta, P. Rocca, M. Bartolomei, M. Lopera Sierra, M. Cremonesi, M. Chinol, H.R. Macke, G. Paganelli, Cancer Biother. Radiopharm. 19 (2004) 65.
[37] F. Iten, B. Muller, C. Schindler, C. Rochlitz, D. Oertli, H.R. Macke, J. Muller-Brand, M.A. Walter, Clin. Cancer Res. 13 (2007) 6696.
[38] I. Virgolini, I. Szilvasi, A. Kurtaran, P. Angelberger, M. Raderer, E. Havlik, F. Vorbeck, C. Bischof, M. Leimer, G. Dorner, K. Kletter, B. Niederle, W. Scheithauer, P. Smith-Jones, J. Nucl. Med. 39 (1998) 1928.
[39] M. de Jong, W.A. Breeman, B.F. Bernard, W.H. Bakker, M. Schaar, A. van Gameren, J.E. Bugaj, J. Erion, M. Schmidt, A. Srinivasan, E.P. Krenning, Int. J. Cancer 92 (2001) 628.
[40] P. Antunes, M. Ginj, H. Zhang, B. Waser, R.P. Baum, J.C. Reubi, H. Maecke, Eur. J. Nucl. Med. Mol. Imaging 34 (2007) 982.
[41] J.C. Reubi, J.C. Schar, B. Waser, S. Wenger, A. Heppeler, J.S. Schmitt, H.R. Macke, Eur. J. Nucl. Med. 27 (2000) 273.
[42] A. Al-Nahhas, Z. Win, T. Szyszko, A. Singh, C. Nanni, S. Fanti, D. Rubello, Anticancer Res. 27 (2007) 4087.
[43] M. Henze, J. Schuhmacher, P. Hipp, J. Kowalski, D.W. Becker, J. Doll, H.R. Macke, M. Hofmann, J. Debus, U. Haberkorn, J. Nucl. Med. 42 (2001) 1053.
[44] S. Froidevaux, A.N. Eberle, M. Christe, L. Sumanovski, A. Heppeler, J.S. Schmiti, K. Eisenwiener, C. Beglinger, H.R. Macke, Intl. J Cancer 98 (2002) 930.
[45] N. Viola-Villegas, A. Vortherms, R.P. Doyle, Drug Target Insights 3 (2008) 13.
[46] L.M. De Leon-Rodriguez, Z. Kovacs, Bioconjug. Chem. 19 (2008) 391.
[47] D. Parker, H. Puschmann, A.S. Batsanov, K. Senanayake, Inorg. Chem. 42 (2003) 8646.
[48] L. Camera, S. Kinuya, K. Garmestani, C. Wu, M.W. Brechbiel, L.H. Pai, T.J. McMurry, O.A. Gansow, I. Pastan, et al., J. Nucl. Med. 35 (1994) 882.
[49] L.L. Chappell, D. Ma, D.E. Milenic, K. Garmestani, V. Venditto, M.P. Beitzel, M.W. Brechbiel, Nucl. Med. Biol. 30 (2003) 581.
[50] M. de Visser, P.J.J.M. Janssen, A. Srinivasan, J.C. Reubi, B. Waser, J.L. Erion, M.A. Schmidt, E.P. Krenning, M. de Jong, Eur. J. Nucl. Med. Mol. Imaging 30 (2003) 1134.
[51] H. Mohsin, J. Fitzsimmons, T. Shelton, T.J. Hoffman, C.S. Cutler, M.R. Lewis, P.S. Athey, G. Gulyas, G.E. Kiefer, R.K. Frank, J. Simon, S.Z. Lever, S.S. Jurisson, Nucl. Med. Biol. 34 (2007) 493.
[52] F. Benetollo, G. Bombieri, L. Calabi, S. Aime, M. Botta, Inorg. Chem. 42 (2003) 148.
[53] O.P. Anderson, J.H. Reibenspies, Acta Cryst. C: Crystal Struct. Commun. C52 (1996) 792.
[54] E. Csajbok, Z. Baranyai, I. Banyai, E. Bruecher, R. Kiraly, A. Mueller-Fahrnow, J. Platzek, B. Raduechel, M. Schaefer, Inorg. Chem. 42 (2003) 2342.
[55] C.A. Chang, L.C. Francesconi, M.F. Malley, K. Kumar, J.Z. Gougoutas, M.F. Tweedle, D.W. Lee, L.J. Wilson, Inorg. Chem. 32 (1993) 3501.
[56] A. Heppeler, J.P. Andre, I. Buschmann, X. Wang, J.C. Reubi, M. Hennig, T.A. Kaden, H.R. Maecke, Chem. Eur. J. 14 (2008) 3026.
[57] A. Riesen, M. Zehnder, T.A. Kaden, Acta Cryst. C: Crystal Struct. Commun. C47 (1991) 531.
[58] S. Aime, A. Barge, M. Botta, M. Fasano, J.D. Ayala, G. Bombieri, Inorg. Chim. Acta. 246 (1996) 423.
[59] D. Parker, K. Pulukkody, F.C. Smith, A. Batsanov, J.A.K. Howard, J. ChemSoc, Dalton Trans: Inorg. Chem. 1972–1999 (1994) 689.
[60] F. Benetollo, G. Bombieri, S. Aime, M. Botta, Acta Cryst. C: Crystal Struct. Commun. C55 (1999) 353.
[61] L. Burai, E. Toth, G. Moreau, A. Sour, R. Scopelliti, A.E. Merbach, Chemistry 9 (2003) 1394.
[62] S. Aime, A. Barge, F. Benetollo, G. Bombieri, M. Botta, F. Uggeri, Inorg. Chem. 36 (1997) 4287.
[63] P. Laine, A. Gourdon, J.-P. Launay, J.-P. Tuchagues, Inorg. Chem. 34 (1995) 5150.

Fusion Pharmaceuticals, Inc.
Exhibit 1035.019

[64] D. Andrew Knight, J.B. Delehanty, E.R. Goldman, J. Bongard, F. Streich, L.W. Edwards, E.L. Chang, Dalton Trans. (2004) 2006.
[65] P.R. Norman, R.D. Cornelius, J. Am. Chem. Soc. 104 (1982) 2356.
[66] M.G. Kim, M.-s. Kim, S.D. Lee, J Suh, J. JBIC 11 (2006) 867.
[67] J. Suh, S.H. Yoo, M.G. Kim, K. Jeong, J.Y. Ahn, M.-s. Kim, P.S. Chae, T.Y. Lee, J. Lee, J. Lee, Y.A. Jang, E.H. Ko, Angew. Chem. Int. Ed. 46 (2007) 7064.
[68] N.N. Greenwood, A. Earnshaw, Chemistry of elements, 2nd ed., Elsevier Ltd., Burlington, MA, Copyright, 1997.
[69] E.T. Clarke, A.E. Martell, Inorg. Chim. Acta 190 (1991) 37.
[70] S. Chaves, R. Delgado, J.J.R. Frausto Da Silva, Talanta 39 (1992) 249.
[71] E.T. Clarke, A.E. Martell, Inorg. Chim. Acta 190 (1991) 27.
[72] X. Wang, T. Jin, V. Comblin, A. Lopez-Mut, E. Merciny, J.F. Desreux, Inorg. Chem. 31 (1992) 1095.
[73] E. Toth, E. Brucher, I. Lazar, I. Toth, Inorg. Chem. 33 (1994) 4070.
[74] K. Kumar, C.A. Chang, L.C. Francesconi, D.D. Dischino, M.F. Malley, J.Z. Gougoutas, M.F. Tweedle, Inorg. Chem. 33 (1994) 3567.
[75] M. Koudelkova, H. Vinsova, V. Jedinakova-Krizova, J. Chromatogr A 990 (2003) 311.
[76] E. Toth, E. Bruecher, Inorg. Chim. Acta 221 (1994) 165.
[77] W.P. Cacheris, S.K. Nickle, A.D. Sherry, Inorg. Chem. 26 (1987) 958.
[78] S.L. Wu, W.D. Horrocks Jr., J. Chem. Soc. Dalton Trans.: Inorg. Chem. (1997) 1497.
[79] M.F. Loncin, J.F. Desreux, E. Merciny, Inorg. Chem. 25 (1986) 2646.
[80] X. Zhu, S.Z. Lever, Electrophoresis 23 (2002) 1348.
[81] L. Burai, I. Fabian, R. Kiraly, E. Szilagyi, E. Brucher, J. Chem. Soc. Dalton Trans.: Inorg. Chem. (1998) 243.
[82] M. Neves, I. Antunes, A. Majkowska, A. Bilewicz, J. Labelled Comp. Radiopharm. 50 (2007) S266.
[83] G.R. Choppin, J. Alloys Comp. 344 (1–2) (2002) 55.
[84] J.F. Desreux, Inorg. Chem. 19 (1980) 1319.
[85] M.F. Marques, C.F.G.C. Geraldes, A.D. Sherry, A.E. Merbach, H. Powell, D. Pubanz, S. Aime, M. Botta, J. Alloys Comp. 225 (1995) 303.
[86] S. Aime, M. Botta, G. Ermondi, Inorg. Chem. 31 (1992) 4291.

Fusion Pharmaceuticals, Inc.
Exhibit 1035.020